



# Deeper insights into the photoluminescence properties and (photo)chemical reactivity of cadmium red ( $\text{CdS}_{1-x}\text{Se}_x$ ) paints in renowned twentieth century paintings by state-of-the-art investigations at multiple length scales

Letizia Monico<sup>1,2,3,a</sup>, Francesca Rosi<sup>1</sup>, Riccardo Vivani<sup>4</sup>, Laura Cartechini<sup>1</sup>, Koen Janssens<sup>3,5</sup>, Nicolas Gauquelin<sup>6</sup>, Dmitry Chezhganov<sup>6</sup>, Johan Verbeeck<sup>6</sup>, Marine Cotte<sup>7,8</sup>, Francesco d'Acapito<sup>9</sup>, Lucrezia Barni<sup>2</sup>, Chiara Grazia<sup>1,2</sup>, Luciano Pensabene Buemi<sup>10</sup>, Jean-Louis Andral<sup>11</sup>, Costanza Miliani<sup>12</sup>, Aldo Romani<sup>1,2,b</sup>

<sup>1</sup> SCITEC - Istituto di scienze e tecnologie chimiche “Giulio Natta”, CNR, Via Elce di Sotto 8, 06123 Perugia, Italy

<sup>2</sup> Centre of Excellence SMAArt and Department of Chemistry, Biology and Biotechnology, University of Perugia, Via Elce di Sotto 8, 06123 Perugia, Italy

<sup>3</sup> AXIS Research Group, NANOLab Centre of Excellence, Department of Physics, University of Antwerp, Groenenborgerlaan 171, 2020 Antwerp, Belgium

<sup>4</sup> Pharmaceutical Science Department, University of Perugia, Via del Liceo 1, 06123 Perugia, Italy

<sup>5</sup> Rijksmuseum, Conservation and Restoration—Scientific Research, Hobbemastraat 22, 1071 ZC Amsterdam, The Netherlands

<sup>6</sup> Electron Microscopy for Materials Research (EMAT), Department of Physics, University of Antwerp, Groenenborgerlaan 171, 2020 Antwerp, Belgium

<sup>7</sup> ESRF, Avenue des Martyrs 71, 38000 Grenoble, France

<sup>8</sup> LAMS, CNRS UMR 8220, Sorbonne Université, UPMC Univ Paris 06, Place Jussieu 4, 75005 Paris, France

<sup>9</sup> IOM-OGG, Istituto Officina dei Materiali, CNR, c/o ESRF, Avenue des Martyrs 71, 38000 Grenoble, France

<sup>10</sup> Peggy Guggenheim Collection, Palazzo Venier dei Leoni, Dorsoduro 701, 30123 Venice, Italy

<sup>11</sup> Musée Picasso, Château Grimaldi, Place Mariejol, 06600 Antibes, France

<sup>12</sup> ISPC - Istituto di Scienze del Patrimonio Culturale, CNR, Via Cardinale Guglielmo Sanfelice 8, 80134 Naples, Italy

Received: 31 October 2021 / Accepted: 3 February 2022

© The Author(s) 2022

**Abstract** Cadmium red is the name used for denoting a class of twentieth century artists' pigments described by the general formula  $\text{CdS}_{1-x}\text{Se}_x$ . For their vibrant hues and excellent covering power, a number of renowned modern and contemporary painters, including Jackson Pollock, often used cadmium reds. As direct band gap semiconductors,  $\text{CdS}_{1-x}\text{Se}_x$  compounds undergo direct radiative recombination (with emissions from the green to orange region) and radiative deactivation from intragap trapping states due to crystal defects, which give rise to two peculiar red-NIR emissions, known as deep level emissions (DLEs). The positions of the DLEs mainly depend on the Se content of  $\text{CdS}_{1-x}\text{Se}_x$ ; thus, photoluminescence and diffuse reflectance vis-NIR spectroscopy have been profitably used for the non-invasive identification of different cadmium red varieties in artworks over the last decade. Systematic knowledge is however currently lacking on what are the parameters related to intrinsic crystal defects of  $\text{CdS}_{1-x}\text{Se}_x$  and environmental factors influencing the spectral properties of DLEs as well as on the overall (photo)chemical reactivity of cadmium reds in paint matrixes. Here, we present the application of a novel multi-length scale and multi-method approach to deepen insights into the photoluminescence properties and (photo)chemical reactivity of cadmium reds in oil paintings by combining both well established and new non-invasive/non-destructive analytical techniques, including macro-scale vis-NIR and vibrational spectroscopies and micro-/nano-scale advanced electron microscopy mapping and X-ray methods employing synchrotron radiation and conventional sources. Macro-scale vis-NIR spectroscopy data obtained from the in situ non-invasive analysis of nine masterpieces by Gerardo Dottori, Jackson Pollock and Nicolas de Staël allowed classifying the  $\text{CdS}_{1-x}\text{Se}_x$ -paints in three groups, according to the relative intensity of the two DLE bands. These outcomes, combined with results from micro-/nano-scale electron microscopy mapping and X-ray analysis of a set of  $\text{CdS}_{1-x}\text{Se}_x$  powders and artificially aged paint mock-ups, indicated that the relative intensity of DLEs is not affected by the morphology, microstructure and local atomic environment of the pigment particles but it is influenced by the presence of moisture. Furthermore, the extensive study of artificially aged oil paint mock-ups permitted us to provide first evidence of the tendency of cadmium reds toward photo-degradation and to establish that the conversion of  $\text{CdS}_{1-x}\text{Se}_x$  to  $\text{CdSO}_4$  and/or oxalates is triggered by the oil binding medium and moisture level and depends on the Se content. Based on these findings, we could interpret the localized presence of  $\text{CdSO}_4$  and cadmium oxalate as alteration products of the original cadmium red paints in two paintings by Pollock.

<sup>a</sup> e-mail: [letizia.monico@cnr.it](mailto:letizia.monico@cnr.it) (corresponding author)

<sup>b</sup> e-mail: [aldo.romani@unipg.it](mailto:aldo.romani@unipg.it) (corresponding author)

## 1 Introduction

Cadmium sulfide and cadmium selenide belong to the II–VI group of semiconductors with a direct bandgap at 2.4 eV and 1.74 eV, respectively. In the last decades there has been a growing interest for their ternary solid solutions,  $\text{CdS}_{1-x}\text{Se}_x$ , since the variation of the Se content offers the possibility to gradually tune the band gap between those of the CdS and CdSe end-members [1–4]. Besides their recent use mainly as optoelectronic and nonlinear optical devices as well as cut-off filters [5–9],  $\text{CdS}_{1-x}\text{Se}_x$  have found applications as artists' pigments during the twentieth century [10]. Cadmium red is the name used for denoting this class of pigments. The color of cadmium reds ranges from orange to purplish red with increasing Se content [2]. For their bright shades and excellent covering power, cadmium reds were largely used by a number of renowned modern and contemporary painters, including Piet Mondrian (1872–1944) [11, 12], Pablo Picasso (1881–1973) [13, 14], Gerardo Dottori (1884–1977) [15, 16], Joan Miró (1893–1983) [17], Jackson Pollock (1912–1956) [18, 19], Nicolas de Staël (1914–1955) [20], Alberto Burri (1915–1995) [21, 22]. They were often used for restoration purposes too [23, 24].

Such class of pigments was firstly commercialized in 1910 with a manufacturing process based on the calcination of a mixture of cadmium sulfide, metallic selenium and elemental sulfur at  $\sim 600^\circ\text{C}$ . Later, in 1919, a second method of synthesis was developed, based on the precipitation of a yellow compound from a solution of alkaline sulfides and selenides, and then converted to red by calcination at  $\sim 300^\circ\text{C}$  [10]. Another procedure, aimed at lowering the manufacturing costs, was introduced in 1921 via the co-precipitation of  $\text{CdS}_{1-x}\text{Se}_x$  with  $\text{BaSO}_4$ . These latter pigments are known as cadmium red lithopones [25, 26].

As direct band gap semiconductors, cadmium reds exhibit direct radiative recombination, with emissions of photons (known as near band edge emission, NBE) in the 530–630 nm range that have energies comparable to the optical band gap. They can also undergo to radiative deactivation from intragap trapping states that are usually related to crystal defects. Such red to near infrared emission bands (positioned in the 780–1100 nm range) are defined as the deep level emissions (DLEs) [2, 3, 27]. The positions of the NBE and of the two DLE bands as well as that of the inflection point of the diffuse reflectance visible spectra depend among other on the Se content of the cadmium red pigment itself. Therefore, photoluminescence and reflectance vis–NIR spectroscopy have been successfully used as diagnostic techniques for the characterization of different types of cadmium reds in artworks [2, 15, 16, 18, 27, 28]. The origin of the DLE bands and the factors affecting their relative intensity is however still a matter of debate. Babentsov et al. [29] have tentatively attributed the presence of the two DLE bands to two different types of cation–anion divacancies ( $V_{\text{Cd}} - V_{\text{Se}}$ ) in CdSe: one type oriented along the hexagonal *c*-axis ( $\text{DLE}_1$ ) and the other oriented along the basal Cd–Se bond directions ( $\text{DLE}_2$ ). Other studies have instead assumed that the occurrence and relative intensity of the  $\text{DLE}_1$  and  $\text{DLE}_2$  bands is attributable to the concentration of lattice-vacancy type defects ( $V_{\text{Se}}$ ) and oxygen-containing species incorporated in the vacancies, respectively [30, 31].

In the last years, vis–NIR spectroscopy along with micro-Raman spectroscopy and X-ray powder diffraction (XRPD) has also been successfully exploited for the study of the stoichiometry and crystalline structure of cadmium yellows (CdS and  $\text{Cd}_{1-x}\text{Zn}_x\text{S}$ ), a class of pigments known for their tendency to undergo discoloration [24, 32–36]. Among the causes of degradation, FT-IR spectroscopy and synchrotron radiation (SR)-based X-ray methods have permitted to demonstrate that: (i) the photo-oxidation of CdS-based compounds to  $\text{CdSO}_4/\text{CdSO}_4 \cdot \text{H}_2\text{O}$  is triggered by the presence of moisture; (ii) the process is more pronounced for  $\text{Cd}_{1-x}\text{Zn}_x\text{S}$  solid solutions with respect to CdS; (iii) the alteration of CdS may also occur in the absence of light, by exposing the paint to high moisture conditions and when chloride species (related to the manufacturing process of the pigment) are present [24, 37].

The alteration of CdSe-compounds has previously been investigated in the field of semiconductor materials and environmental chemistry. Studies established that during irradiation of CdSe nanocrystals in aerobic conditions, photo-oxidation occurs by producing cadmium oxide and selenium dioxide [38, 39]. In aqueous environments, it has been observed that the photo-dissolution of  $\text{CdS}_{1-x}\text{Se}_x$  can lead to the formation of sulfate- and selenate-based compounds [40]. In the field of heritage science, the discoloration of  $\text{CdS}_{1-x}\text{Se}_x$  has been documented recently only in an ancient Greek terracotta krater, where the pigment was used as a restoration material. In this specific case, light and chlorine species were identified as two possible triggering factors of the alteration process [41].

Based on the extensive use of  $\text{CdS}_{1-x}\text{Se}_x$  pigments in twentieth century oil paintings [11–15, 17–21], it becomes highly relevant to develop a methodological strategy that allows deeper understanding of the intrinsic properties of  $\text{CdS}_{1-x}\text{Se}_x$  and environmental factors influencing the photoluminescence and the (photo)chemical stability of cadmium reds in oil. The ultimate goal of this research is to contribute to the preservation of unique masterpieces containing cadmium red pigments.

Here, we benefitted from a combination of macro-scale *in situ* non-invasive vis–NIR and reflection FT-IR spectroscopy to obtain a complete overview of the composition and current condition of different  $\text{CdS}_{1-x}\text{Se}_x$ -based paints used throughout a series of renowned twentieth century oil paintings (nine in total) by Gerardo Dottori, Jackson Pollock and Nicolas de Staël. These results were then compared with outcomes arising from the study of a series of  $\text{CdS}_{1-x}\text{Se}_x$  pigment powders with different photoluminescence properties and Se content and from a set of cadmium red-based oil paint mock-ups aged under controlled conditions of light and moisture. On the one hand, high-angle annular dark-field scanning transmission electron microscopy (HAADF-STEM) and energy dispersive X-ray (EDX) spectroscopy mapping techniques jointly with XRPD and X-ray absorption spectroscopy (XAS) at S K-, Cd L<sub>3</sub>- and Se K-edges permitted to obtain micro-/nano-scale information on some intrinsic properties of  $\text{CdS}_{1-x}\text{Se}_x$  pigment powders, including their elemental composition, morphology, microstructure and local atomic environment. On the other

hand, vis–NIR spectroscopy, FT-IR spectroscopy and XRPD investigations provided an in-depth characterization at the millimetric scale of the optical and molecular modifications induced by the artificial aging treatments of paint mock-ups. These analyses offered new insights into the external circumstances and internal factors influencing the photoluminescence properties and (photo)chemical reactivity of cadmium red paints.

## 2 Materials and methods

### 2.1 Case studies

The following twentieth century oil paintings were selected as case studies:

- i. *Incendio Città* (1926; oil on canvas) and *Lago Umbro* (1942; oil on panel) by Gerardo Dottori, belonging to the Collection of Civic Museum of Palazzo della Penna of Perugia, Italy;
- ii. *The Moon Woman* (1942; oil on canvas), *Direction* (1945; oil on canvas), *Circumcision* (1946; oil on canvas), *Bird Effort* (1946; oil on canvas), *Eyes in the Heat* (1946; oil and alkyd enamel on canvas) and *Alchemy* (1947; oil, aluminum, alkyd enamel paint with sand, pebbles, fibres, and wood on commercially printed fabric) by Jackson Pollock, owned by the Peggy Guggenheim Collection of Venice, Italy;
- iii. *Le Concert* (1955; oil on canvas) by Nicolas de Staël, belonging to the Musée Picasso of Antibes, France.

All artworks were analyzed in situ without moving the painting from their exhibition room. For the nine paintings cited above, a total of more than n. 70 reflectance FT-IR spectra and n. 100 reflectance and fluorescence UV–vis–NIR spectra were collected from spots of selected red areas.

### 2.2 Commercial and historical $\text{CdS}_{1-x}\text{Se}_x$ pigments and preparation of oil paint mock-ups

Four  $\text{CdS}_{1-x}\text{Se}_x$  pigment powders commercially available by Kremer GmbH (Germany) were investigated and used for preparing a set of oil paint mock-ups. Further information on the optical and vibrational spectroscopy properties as a function of the pigment composition are reported elsewhere [2]. Samples are named according to the Kremer catalog (21080, 21110, 21130, 21150). The set of historical  $\text{CdS}_{1-x}\text{Se}_x$  pigments, always produced by Kremer GmbH, was composed of five powders dated back to *ca.* 1960–1970. Such compounds, belonging to the collection of the Center for Art Technological Studies (CATS) of the Statens Museum for Kunst in Copenhagen (Denmark), are named throughout the paper according to CATS database list (437, 439, 440, 442, 565). In the sample name, the subscript “Se = numerical value” stands for the Se/(Se + S) molar ratio, which equals to the x value in the  $\text{CdS}_{1-x}\text{Se}_x$  formula, obtained via XRPD (*cf.* Table 1). This ratio will be indicated as  $x_{\text{Se}}$  throughout the text.

**Table 1** XRPD results of commercial and historical  $\text{CdS}_{1-x}\text{Se}_x$  pigment powders. Refined unit cell parameters, site occupancy factor for Se ( $x_{\text{Se}}$ ), isotropic microstructural data in terms of size of coherent domains (volume-weighted) ( $D_v$ ) and microstrain as % of average unit cell deformation ( $\varepsilon$ ), and phase wt% obtained by means of the Rietveld method

Sample	$a$ (Å)	$c$ (Å)	$x_{\text{Se}}$	$D_v$ (nm) <sup>a</sup>	$\varepsilon$ (%) <sup>a</sup>	wt% <sup>b</sup>
21080	$4.1591 \pm 0.0001$	$6.7578 \pm 0.0001$	$0.14 \pm 0.01$	171	0.22	$97.5 \pm 0.5$
21100	$4.1723 \pm 0.0001$	$6.7824 \pm 0.0001$	$0.22 \pm 0.01$	210	0.57	100
21130-I	$4.1956 \pm 0.0001$	$6.8257 \pm 0.0002$	$0.36 \pm 0.01$	292 <sup>c</sup>	0.33 <sup>c</sup>	$28.8 \pm 0.5$
21130-II	$4.2017 \pm 0.0001$	$6.8357 \pm 0.0001$	$0.40 \pm 0.01$	292 <sup>c</sup>	0.33 <sup>c</sup>	$71.2 \pm 0.5$
21150-I	$4.2107 \pm 0.0001$	$6.8511 \pm 0.0002$	$0.45 \pm 0.01$	309 <sup>d</sup>	0.39 <sup>d</sup>	$34.9 \pm 0.5$
21150-II	$4.2270 \pm 0.0001$	$6.8800 \pm 0.0002$	$0.55 \pm 0.01$	309 <sup>d</sup>	0.39 <sup>d</sup>	$58.0 \pm 0.5$
437	$4.1569 \pm 0.0001$	$6.7561 \pm 0.0002$	$0.12 \pm 0.01$	132	0.15	$96.5 \pm 0.5$
439	$4.1934 \pm 0.0001$	$6.8217 \pm 0.0001$	$0.38 \pm 0.02$	162	0.14	$96.2 \pm 0.5$
440	$4.2096 \pm 0.0001$	$6.8514 \pm 0.0001$	$0.47 \pm 0.02$	206	0.21	100
442-I	$4.1666 \pm 0.0001$	$6.7745 \pm 0.0002$	$0.19 \pm 0.01$	87	0.16	$41.0 \pm 0.5$
442-II	$4.2245 \pm 0.0001$	$6.8771 \pm 0.0002$	$0.54 \pm 0.01$	525	0.50	$57.2 \pm 0.5$
565-I	$4.1563 \pm 0.0003$	$6.7519 \pm 0.0007$	$0.11 \pm 0.06$	170	0.11	$3 \pm 1$
565-II	$4.1980 \pm 0.0001$	$6.8281 \pm 0.0001$	$0.40 \pm 0.01$	165	0.20	$67 \pm 1$

<sup>a</sup>Uncertainties can be estimated as 10% of the reported values

<sup>b</sup>The complement to 100 is  $\text{BaSO}_4$  for all samples

<sup>c,d</sup> Constrained values due to strong peak overlap

Oil paint mock-ups were prepared by following the same approach earlier used for obtaining a series of cadmium yellow mock-ups [24, 37]. Notably, commercial powders were mixed with cold pressed linseed oil (Zecchi, Italy) in a 4:1 mass ratio and applied on polycarbonate slices. Samples were left to dry at environmental conditions (RH: ~30%; temperature: ~20 °C) for about 1 month.

To evaluate the photochemical response of  $\text{CdS}_{1-x}\text{Se}_x$  pigments in the absence of linseed oil, the commercial powders were also prepared in the form of concentrated pellets, obtained using a hydraulic press. The mechanic resistance of each pellet was guaranteed by embedding them in a polyester resin block. One of the faces of the pellet was left exposed to make aging and measurements possible. It should be noted that all pellets show the same spectral features of the corresponding raw powders; therefore, it can be excluded any meaningful change induced by the pressure in the original properties of the pigments. In addition, it is reasonable to assume that the packaging of the powder has not a significant contribution on the overall photochemical reactivity of the pigment.

The list of commercial and historical pigments along with the corresponding oil paint mock-ups, are reported in Tables 1 and 3.

### 2.3 Artificial aging protocols

UVA-visible photochemical aging treatments of oil paint mock-ups and pigment pellets were performed using an in-house made aging chamber equipped with a UV-filtered 300 W Cermax xenon lamp simulating the museum indoor lighting environment ( $\lambda \geq 300$  nm; see ref [42] for its emission spectral profile) either at RH of ~30% (measured indoor humidity level) or at RH  $\geq 95\%$ . The irradiance and temperature, measured at each sample position, were  $0.7 \div 1 \times 10^3$  W/m<sup>2</sup> and 31 °C, respectively. Samples were irradiated for  $480 \div 504$  h such to achieve total irradiance exposure values of  $3 \div 5 \times 10^5$  W/m<sup>2</sup>·h.

Thermal aging treatments were carried out by allocating the touch-dry paints (i.e., after about one month since their preparation) in a sealed vessel kept at RH  $\geq 95\%$  with distilled water. The vessel was maintained in the oven at ~40 °C for an overall period of 21 days (504 h).

The aging conditions, selected also on the basis of previous studies [37], were aimed at evaluating the separate and joint effect of UVA-visible light and climate parameters (i.e., moisture and temperature) on the overall degradation pathways of cadmium reds.

### 2.4 UV-vis-NIR spectroscopy

Reflection and fluorescence UV-vis-NIR investigations at selected spots of paintings, cadmium red pigment powders and paint mock-ups were performed by a self-assembled portable instrument. A deuterium-halogen lamp (AvaLight-DHc, Avantes), a highly sensitive charge-coupled device (CCD) spectrometer (AvaSpec-2048 USB2, Avantes; 200–1100 nm range; 8 nm spectral resolution) and a thermoelectrically cooled InGaAs detector (AvaSpec-NIR256-1.7TEC; 950–1600 nm range; 24 nm spectral resolution) were used for carrying out reflection measurements. An ultracompact diode laser (Toptica Photonics AG, DE; 445 nm excitation wavelength, 1 mW nominal power), integrated into the same apparatus and coupled with two high-sensitivity calibrated CCD spectrometers (i.e., AvaSpec-NIR256-1.7TEC and AvaSpec-ULS2048 XL-RS-USB2; 300–1150 nm range; 9.2 nm spectra resolution), was used for performing photoluminescence measurements. The instrument has a dedicated fiber-optic system, designed to direct all the excitation sources to the same point of the analyzed surface and, at the same time, collect both the reflected and emitted light, bringing them to the different detectors. The probe area is less than 2 mm<sup>2</sup>.

Reflectance and fluorescence spectra were recorded using an integration time of 800 ms and 500 ms, respectively, and with 30 averages. Band gap energies were determined from reflectance spectra as earlier described by Grazia et al. [2] (see also Sect. 5 of the Supplementary Information for further details). Fluorescence spectra were processed by employing a curve-fit procedure with Gaussian functions to get accurate values for the emission band maxima (see Supplementary Information: Fig. S1 and Table S1). These values were used for an approximate estimation of  $x_{\text{Se}}$  and have been used for the comparison of the results obtained from the case studies with a series of  $\text{CdS}_{1-x}\text{Se}_x$  pigments also characterized by XRPD. For the commercial cadmium reds, slight differences are observed in the DLE maxima positions in the wavelength scale with respect to earlier research [2] since the spectra were fitted without applying the Jacobian transformation, which allows obtaining a more accurate value of the energies in eV.

### 2.5 HAADF-STEM/STEM-EDX mapping

TEM lamellas were prepared by focused ion beam (FIB) technique from the two commercial powders 21080 and 21150 and the two historical powders 437 and 442 dispersed on a carbon tape. After carbon coating, the surface was further coated with platinum and the specimen was subsequently cut as a lamella and thinned between 50 and 100 nm using FIB. The obtained FIB lamellas were then analyzed by EDX using a 50 pA beam current to limit beam damage on a STEM Thermofisher scientific Titan 60-30, operating at 300 kV and equipped with a high efficiency Super-X detector. The elemental quantitative analysis was performed using the embedded routine in the Bruker Esprit software. Each powder was imaged in a Thermofisher scientific QUANTA FEG 250 at the accelerating voltage of 20 kV in secondary electron detection mode. The particle size analysis was made by means of Fiji (ImageJ) software [43] using SEM images.

## 2.6 XRPD and Rietveld refinements

XRPD patterns for qualitative phase analysis and Rietveld refinements were collected from cadmium red pigment powders [mixed with silicon (~ 20 wt. %) as internal line position standard] and paint mock-ups by the Cu-K $\alpha$  radiation on a PANalytical X'PERT PRO diffractometer and PW3050 goniometer, equipped with an X'Celerator detector. The long fine focus ceramic tube worked at 40 kV and 40 mA. The instrumental contribution to the peak shape was evaluated before measuring samples by the Rietveld refinement of lanthanum hexaboride (LaB $_6$ ) as an external peak profile standard.

Structural and microstructural information of pigment powders were obtained by the Rietveld refinement of XRPD patterns using modified pseudo-Voigt functions of the GSAS-EXPGUI package [44] and by following the procedure described elsewhere [45]. Unit cell parameters, sample displacement, background and profile were first refined. Following, atomic coordinates, atomic displacement parameters and site occupancy factors for S and Se were also refined. Eventual preferred orientations of microcrystals were corrected by expanding the orientation distribution in spherical harmonics. The iterative refinement procedure was stopped when the shifts in all parameters were less than their standard deviations. Since S and Se are randomly distributed in the same crystallographic site, the site occupancy factor for Se, estimated by the Rietveld refinement procedure, is equal to the  $x$  value in the of CdS $_{1-x}$ Se $_x$  formula (denoted as “ $x_{Se}$ ”; see also par. 2.2).

Refinements were carried out using both isotropic and anisotropic models, this last assuming [001] as the broadening axis, from which different size and microstrain values in two directions, parallel and normal to this axis, could be determined. However, since the two models provided very similar data for all samples, only the results yielded by the isotropic model are reported for sake of simplicity (cf. Table 1). The coherent domain sizes (volume-weighted,  $D_v$ ) and microstrain values ( $\varepsilon$ ) were estimated using Eqs. 1 and 2, respectively:

$$D_v = 1800\lambda/\pi X \quad (1)$$

$$\varepsilon = (\pi/18000)(Y - Yi) \quad (2)$$

where  $X$ , and  $Y$  are the refined peak shape parameters, whereas  $Yi$  is the instrumental contribution.

## 2.7 XAS at S K-, Cd L $_3$ - and Se K-edges

XAS investigations at S K-, Cd L $_3$ - and Se K-edges of a selection of commercial and historical CdS $_{1-x}$ Se $_x$  pigment powders were performed at the scanning x-ray microscope end station of beamline ID21 and at the beamline BM08-LISA of the European Synchrotron Radiation Facility (ESRF, Grenoble, France) using the recently installed Extremely Brilliant Source (EBS) [46–48]. Measurements were carried out by means of a Si(111) and a Si(311) double-crystal monochromator, at ID21 and BM08-LISA, respectively. At these beamlines, single point XAS spectra were recorded in transmission mode under vacuum conditions and a beam with sizes ( $h \times v$ ) of  $300 \times 300 \mu\text{m}^2$  and  $\sim 70 \times 200 \mu\text{m}^2$ , respectively.

At ID21 data were recorded via the new-developed Daiquiri web-based user interface framework [49] from a thin layer of powder fixed on S-free tape, by scanning the primary energy around the S K-edge (from 2.45 to 2.65 keV range; energy step: 0.2 eV) and Cd L $_3$ -edge (from 3.51 to 3.65 keV; energy step: 0.3 eV) and using a photodiode as detector. At BM08-LISA spectral profiles were collected using ion chambers filled with N $_2$  gas. Pellets, were prepared by mixing about 33 mg of cellulose with 22–28 mg of sample and by scanning the primary energy around the Se K-edge with the following steps: (i) 12.4648–12.6388 keV, step: 5 eV; (ii) 12.6438–12.7227 keV, step: 0.5 eV; (iii) 12.7232–13.9016 keV, step: from 2 to 7 eV. The energy calibration was performed using CaSO $_4 \cdot 2\text{H}_2\text{O}$ , and a Se foil as standards. At ID21, the energy calibration was performed using CaSO $_4 \cdot 2\text{H}_2\text{O}$  (maximum of the white line at 2.4826 keV) and a Cd foil for the S K- and Cd L $_3$ -edges investigations, respectively. In the case of BM08-LISA beamline, a grey Se sample was employed as a calibrant and a spectrum was collected at the same time as the sample in order to guarantee the energy scale stability, which resulted to be better than 0.01 eV.

The ATHENA [50] code was used for the normalization and the processing of the XAS data and the ARTEMIS code for the quantitative fitting. Theoretical extended X-ray absorption fine structure (EXAFS) paths were generated with the FEFF8.4 code [51] from a cluster of sphalerite CdS $_{0.5}$ Se $_{0.5}$ , simulated using Density Functional Theory (DFT) as implemented in the VASP code [52]. This structure was chosen as it bears similar electron density and bond length values as the wurtzite-type structure while resulting easier to relax with DFT. The data were fitted by means of a multishell model consisting in a first Se-Cd shell with 4 neighbours, a second Se-(Se, S) shell composed of 12 neighbours with a variable Se content and a third shell made up of 12 Cd atoms.

Being a series of pigments sensitive towards exposure to SR-based X-ray beams [53–56], preliminary tests at variable fluences and/or exposure times were performed at a few spots of each analyzed powders to ensure that the collected data were not affected by any artefacts due to X-ray beam exposure.

## 2.8 Colorimetry

Investigations of color changes of paint mock-ups were performed by a Konica-Minolta CM700D portable colorimeter. The instrument is provided of a pulsed xenon lamp emitting in the visible spectral range, a silicon photodiode array detector and an inte-



grating sphere with a 40 mm internal diameter. The software interfaced with the colorimeter allowed for the conversion of the spectra (acquired in the 360–740 nm range and with 10 nm spectral resolution) into CIE  $L^*a^*b^*$  chromatic coordinates under the D65 standard illuminant and 10° angle observer. Total color changes were calculated according to the CIE 1976 formula,  $\Delta E^* = (\Delta L^{*2} + \Delta a^{*2} + \Delta b^{*2})^{1/2}$ .

## 2.9 FT-IR spectroscopy

A portable ALPHA spectrometer (Bruker) was used for carrying out attenuated total reflection (ATR) mode measurements at the surface of the unaged/aged cadmium red oil paint mock-ups and no contact external reflection mode investigations at selected spots of the cadmium red pellets and in situ directly on paintings.

ATR spectra were recorded using a Platinum QuickSnap ATR sampling module (A220/D-01) equipped with a diamond crystal plate. Data were recorded in the 4000–320  $\text{cm}^{-1}$  range, with 4  $\text{cm}^{-1}$  spectral resolution and 168 scans. It is worth underlining that, although the ATR spectra should be nearly identical to those recorded in transmission mode, some of the most intense vibrational modes of the analyzed compounds appear distorted and slightly shifted in wavenumber positions. This feature is probably due to the fact that in correspondence to strongly adsorbing bands there is a sharp rise in refractive index of the material that may determine the criterion of internal reflection to be lost [57]. Hence, aged-induced changes of some vibrational modes (e.g., CO ester asymmetric stretching of linseed oil) were troublesome to be accurately evaluated in the ATR mode.

Pseudo-absorbance spectra [ $\text{Log}(1/R)$ ;  $R$  is reflectance] were obtained using an external reflection module from areas of about 7  $\text{mm}^2$ . Data were acquired in the 7400–345  $\text{cm}^{-1}$  range, at a resolution of 4  $\text{cm}^{-1}$  and for 3 min.

## 3 Results and discussion

### 3.1 Characterization of cadmium red paints in twentieth century paintings

A selection of the vis–NIR spectroscopy results obtained from cadmium red paints of nine paintings during non-invasive analytical MOLAB campaigns held at the Civic Museum of Palazzo della Penna (Perugia, Italy), the Peggy Guggenheim Collection (Venice, Italy) and the Musée Picasso (Antibes, France) over the last decade is presented in Fig. 1. It is relevant to highlight that, XRF measurements (results not reported) show the presence of cadmium and selenium in all the described paints.

Depending on the analyzed areas, spectra show shifts in the position of both the inflection point of the reflectance vis spectra (Fig. 1a) and the two DLE bands of the emission profiles (Fig. 1b). Conforming to previous research [2, 16], these shifts in position can be exploited for the identification of cadmium reds with different Se content. Under the employed experimental conditions, no accurate information is instead obtainable through analysis of the NBE band located in the visible range (below 700 nm), overlapping with the emission of the binder that contributes in a variable and not determinable extent to the luminescence [16]. Interestingly, the DLE bands also show variations in their relative intensity, although they present almost the same position in some cases.

Hence, based on the obtained results and comparison with a set of  $\text{CdS}_{1-x}\text{Se}_x$  reference pigments (see Sect. 3.2 for further results about these materials), three types of cadmium red paints, featuring different photoluminescence properties, can be discriminated in the analyzed paintings.

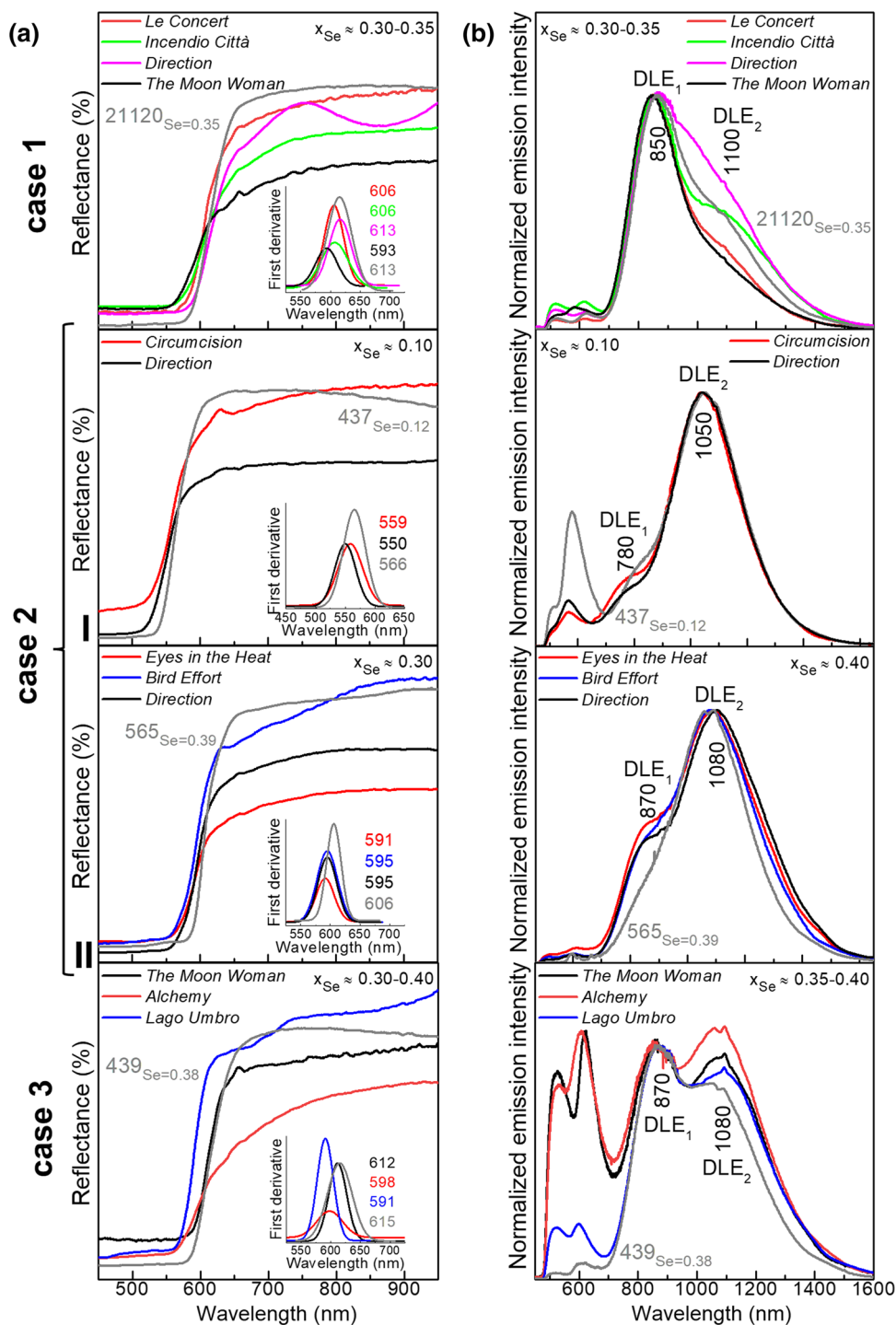
**Case 1.** Some cadmium red-based paints of *Le Concert*, *Incendio Città*, *Direction* and *The Moon Woman* (Supplementary Information: Fig. S2) are characterized by reflectance vis spectra with an inflection point varying in the 593–613 nm range and by emission profiles with a DLE<sub>1</sub> band at around 850 nm, therefore suggesting a  $\text{CdS}_{1-x}\text{Se}_x$  pigment with  $x_{\text{Se}} \approx 0.30\text{--}0.35$  (Fig. 1a). Variations above 600 nm in the reflectance vis spectrum recorded from *Direction* (magenta line) are due to the additional presence of red ochre [58]. In this case, the relative intensity of the DLE bands are very similar to that of the commercial  $\text{CdS}_{1-x}\text{Se}_x$  pigment 21120<sub>Se=0.35</sub>, by featuring an intense DLE<sub>1</sub> band and a weaker shoulder DLE<sub>2</sub> band at around 1100 nm (see ref [2]. for details about the optical properties of the reference pigment).

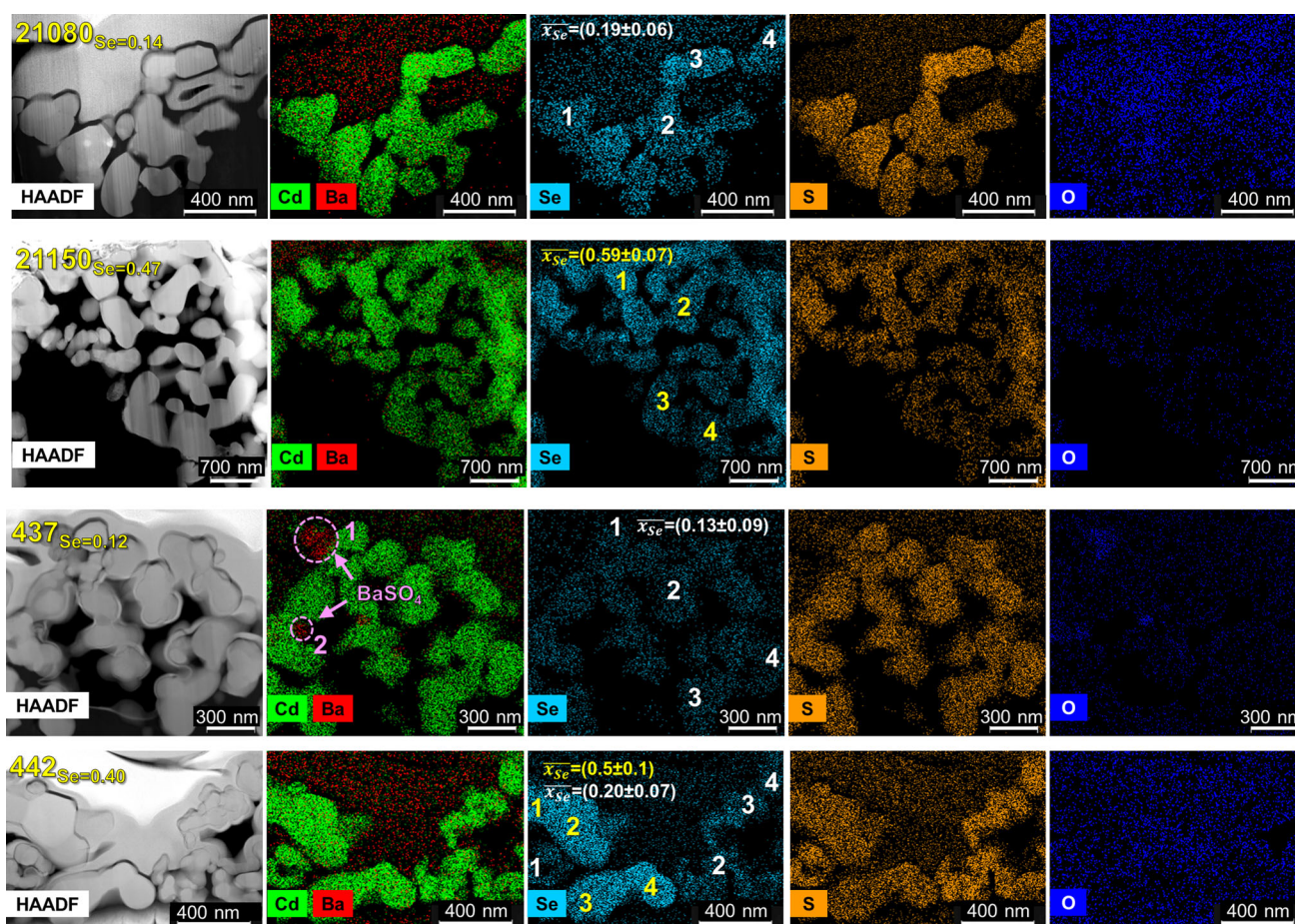
**Case 2.** The group of emission vis–NIR spectra belonging to case 2 reveals instead photoluminescence properties more similar to those of two historical powders (i.e., 437<sub>Se=0.12</sub> and 565<sub>Se=0.39</sub>) (Fig. 1b): the DLE bands feature relative intensities that are inverted with respect to the data of case 1, but, sometimes, with comparable energy positions. The two compositional sub-groups can be distinguished by considering the position of the two DLE bands. The first sub-group (case 2-I) includes the spectra recorded from the red–orange Cd-based paints of *Circumcision* and *Direction* (Supplementary Information: Fig. S3a). Similarly to the spectral profile of the historical powder 437<sub>Se=0.12</sub>, reflectance and emission vis–NIR spectra exhibit an inflection point at 550–559 nm and an intense DLE<sub>2</sub> band at 1050 nm, that are assignable to a  $\text{CdS}_{1-x}\text{Se}_x$  pigment with  $x_{\text{Se}} \approx 0.1$  (Fig. 1). The second sub-group (case 2-II) comprises the spectra obtained from selected red paints of *Eyes in the Heat*, *Bird Effort* and *Direction* (Supplementary Information: Fig. S3b). In these cases, the Se content of the  $\text{CdS}_{1-x}\text{Se}_x$  pigment ( $x_{\text{Se}} \approx 0.30\text{--}0.40$ ) is rather similar to that of case 1, as pointed out by the inflection point at 591–595 nm and the DLE<sub>2</sub> band at 1080 nm in the reflectance and emission vis–NIR profiles (Fig. 1). The slight differences obtained in the  $x_{\text{Se}}$  values from the reflectance and emission vis–NIR spectroscopy measurements (namely  $x_{\text{Se}} \approx 0.3$  and  $x_{\text{Se}} \approx 0.4$ , respectively) are related to the low intensity of the DLE<sub>1</sub> band that affects the curve-fitting results.

**Case 3.** In some cadmium red paints of *The Moon Woman*, *Alchemy* and *Lago Umbro* (Supplementary Information: Fig. S3c) a  $\text{CdS}_{1-x}\text{Se}_x$  pigment with  $x_{\text{Se}} \approx 0.30\text{--}0.40$  was identified too via the presence of an inflection point in the 591–612 nm range in the reflectance vis spectra and a red-NIR fluorescence with DLE<sub>1</sub> and DLE<sub>2</sub> bands at 870 and 1080 nm, respectively (Fig. 1). With respect to the emission vis–NIR data of case 2-II, here, the DLE<sub>1</sub> band has an intensity comparable to that of DLE<sub>2</sub>. Their positions and relative intensities are very similar to those of the historical pigment 439<sub>Se=0.38</sub>.

Overall, the variable relative intensity of the  $\text{CdS}_{1-x}\text{Se}_x$  DLE bands observed in the spectra recorded from the analyzed twentieth century paintings show that other factors than the Se content influence the photoluminescence properties of cadmium reds.

**Fig. 1** **a** Diffuse reflectance vis spectra and **b** normalized emission vis–NIR spectra recorded from selected red paints of the analyzed twentieth century paintings and composed of  $\text{CdS}_{1-x}\text{Se}_x$  pigments with different Se content and photoluminescence properties.  $x_{\text{Se}}$  was estimated from the inflection point of the diffuse reflectance vis spectrum and from the maxima of the DLE<sub>1</sub> band





**Fig. 2** HAADF-STEM images and STEM-EDX maps of (green) cadmium, (red) barium, (cyan) selenium, (orange) sulfur and (blue) oxygen recorded from selected commercial and historical  $\text{CdS}_{1-x}\text{Se}_x$  pigment powders (from top):  $21080_{\text{Se}=0.14}$ ,  $21150_{\text{Se}=0.47}$ ,  $437_{\text{Se}=0.12}$  and  $442_{\text{Se}=0.40}$ . Numbers show the areas where single-points EDX measurements were performed, with  $\overline{x_{\text{Se}}}$  that indicates the average value of  $x_{\text{Se}}$  (for further details about the quantitative results, see Supplementary Information: Table S2)

### 3.2 Internal and external factors affecting the spectral properties of the DLEs in $\text{CdS}_{1-x}\text{Se}_x$

In order to understand the factors influencing the spectral properties of DLE bands, in a first step, we investigated some of the possible parameters related to intrinsic crystal defects of  $\text{CdS}_{1-x}\text{Se}_x$ , including morphology, microstructure and local atomic structure. In a second step, we assessed if/how eventual chemical transformations of  $\text{CdS}_{1-x}\text{Se}_x$  (both in the presence and in the absence of the oil medium) induced by (photo)aging treatments may affect the photoluminescence properties of the pigment itself. Results are described and discussed hereafter.

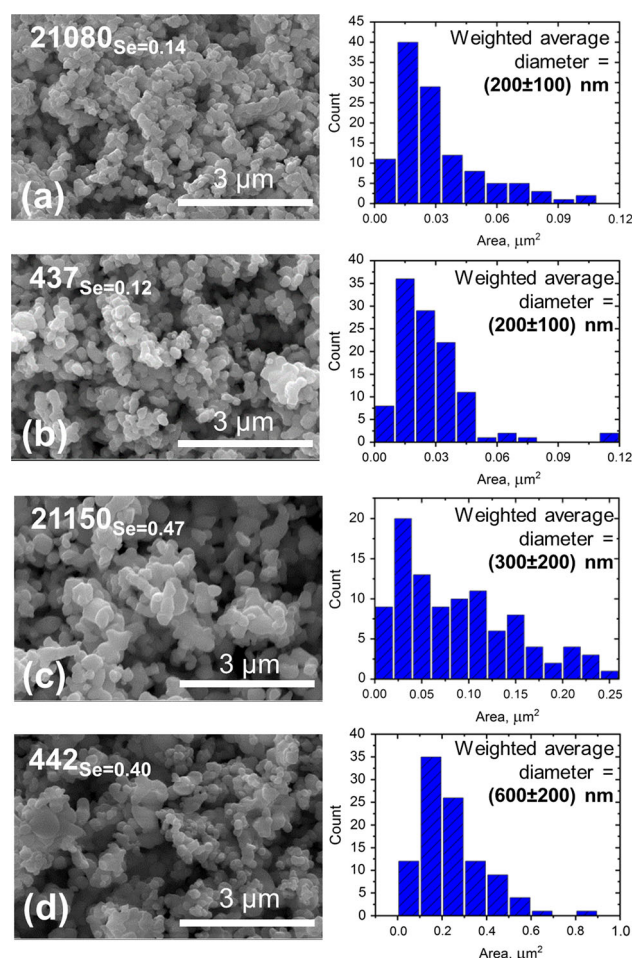
#### 3.2.1 Morphology, microstructure and local atomic structure of $\text{CdS}_{1-x}\text{Se}_x$

HAADF-STEM and STEM-EDX maps (Fig. 2) of historical ( $437_{\text{Se}=0.12}$ ,  $442_{\text{Se}=0.40}$ ) and commercial ( $21080_{\text{Se}=0.14}$ ,  $21150_{\text{Se}=0.47}$ )  $\text{CdS}_{1-x}\text{Se}_x$  pigments, selected for their comparable Se content but with DLE bands featuring opposite relative intensity (*cf.* Figs. 1 and 6b and Supplementary Information: Fig. S4), show a similar elemental distribution, with Cd, S and Se as dominant elements of each particle. The average value of  $x_{\text{Se}}$  (hereinafter defined as “ $\overline{x_{\text{Se}}}$ ”) measured in the  $\text{CdS}_{1-x}\text{Se}_x$  grains is in line with that obtained by XRPD within experimental error (Table 1). Furthermore, no co-localization among  $\text{CdS}_{1-x}\text{Se}_x$  particles and both  $\text{BaSO}_4$  (present in form of particles) and other trace elements, such as Zn, were identified (for further details, see Supplementary Information: Table S2). Thus, also in line with the fact that no changes are observed in the positions of DLE bands in pigments with comparable Se content, it is very likely that the synthesis has not led to the formation of Ba- and/or Zn-doped  $\text{CdS}_{1-x}\text{Se}_x$  particles under any circumstances.

From the morphological and microstructural point of view, average size of particles and crystallites obtained via SEM imaging (Fig. 3) and Rietveld refinement of XRPD patterns (Table 1:  $D_v$ ), respectively, are comparable for all phases with a similar Se content. This result suggests that the extent of particle aggregation/agglomeration can be considered negligible in all powders. Furthermore,



**Fig. 3** SEM images and particle size distribution of selected commercial and historical  $\text{CdS}_{1-x}\text{Se}_x$  pigment powders: **a**  $21080_{\text{Se}=0.14}$ , **b**  $437_{\text{Se}=0.12}$ , **c**  $21150_{\text{Se}=0.47}$  and **d**  $442_{\text{Se}=0.40}$



the average size of particles/crystallites depends on  $x_{\text{Se}}$ , by increasing with increasing degree of Se substitution. Microstrain varies from 0.14 to 0.57% (Table 1:  $\epsilon$ ), by showing in general the same trend for both commercial and historical pigments because of increasing lattice distortions when Se atoms progressively replace the smaller S ones.

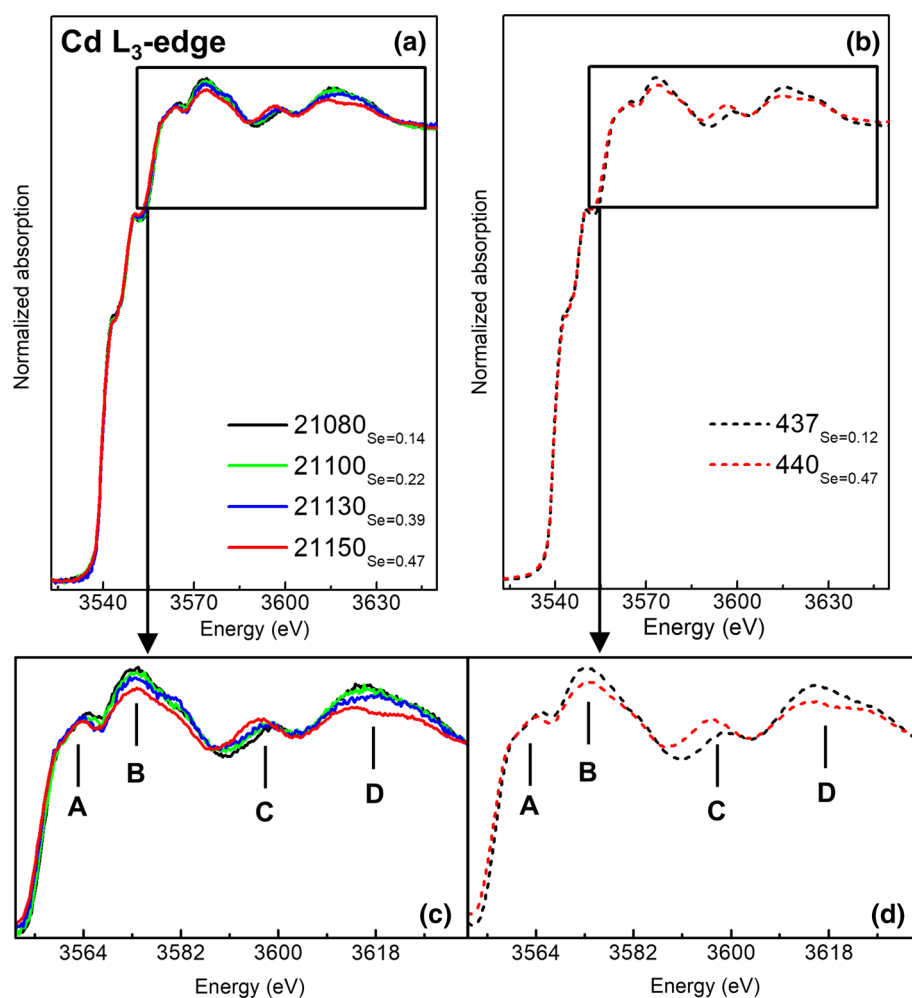
In agreement with earlier studies [59, 60, 60–62] and the XRPD lattice parameters (Table 1), Cd  $L_{3-}/\text{S}$  K-edge XANES spectroscopy analysis (Fig. 4 and Supplementary Information: Fig. S5) combined with Se K-edge EXAFS spectroscopy investigations (Fig. 5 and Supplementary Information: Fig. S6) reveal that the local atomic structure and bonding are dependent on the Se content and that  $\text{CdS}_{1-x}\text{Se}_x$  compounds are in the hexagonal crystalline structure.

The Cd  $L_{3-}$  edge XANES spectra of commercial and historical  $\text{CdS}_{1-x}\text{Se}_x$  with similar Se content are very similar (Fig. 4). Subtle differences are visible only when the Se content increases in  $\text{CdS}_{1-x}\text{Se}_x$ , including a decrease of the intensity of some post-edge features (peaks B, D) and a progressive shift towards lower energies (peaks A, C). Such changes are in line with previous studies on  $\text{CdS}_{1-x}\text{Se}_x$  nanostructures [61, 62]. No meaningful differences are present in the S K-edge spectra, whose analysis is further complicated by the presence of variable amounts of sulfate-species, mainly due to the extenders/additives (Supplementary Information: Fig. S5).

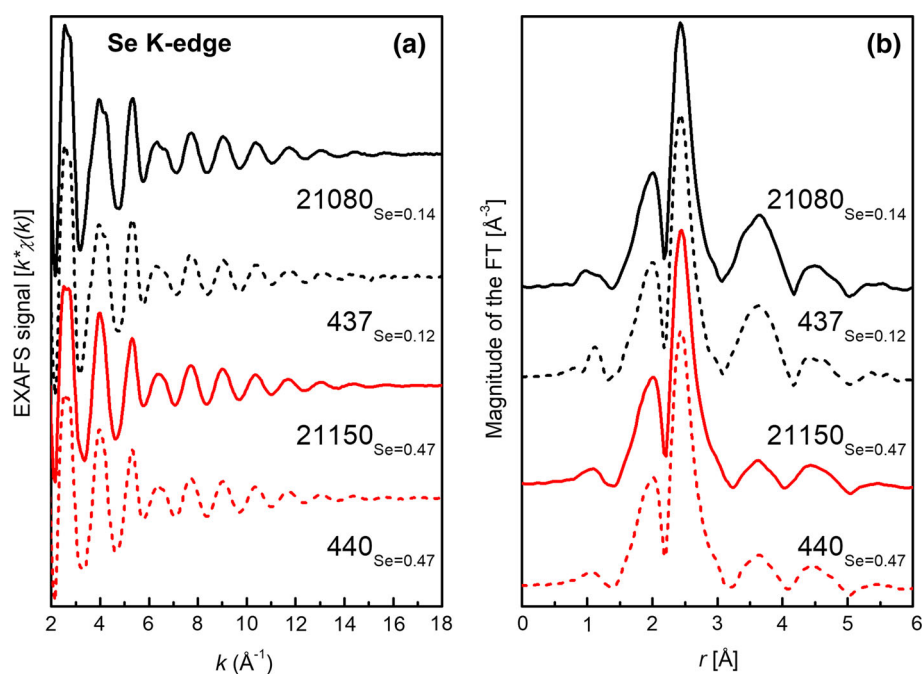
In a similar way, the Se K-edge XANES spectral region (Supplementary Information: Fig. S6) of the Se-poorer compounds  $21080_{\text{Se}=0.14}/437_{\text{Se}=0.12}$  and of the Se-richer pigments  $21150_{\text{Se}=0.47}/440_{\text{Se}=0.47}$  appear similar, meaning that no appreciable differences are visible between samples with a similar Se content. In agreement with earlier studies [61], only a slight shift towards lower energies of the maximum of the white line (between ca.  $-0.20$  and  $-0.14$  eV; see Table S3) is visible with increasing Se content. More revealing information can be obtained by looking at the Se K-edge EXAFS spectra and the related Fourier Transforms (FT) in the 3–4 Å region (Fig. 5), where a less pronounced second shell peak is present in the Se-richer pigments. The quantitative analysis results of the Se K-edge XAS data are presented in Table 2.

In agreement with previous literature [59], the structure found is well described by the employed fit model, which includes 4 Cd neighbours at 2.60 Å, a mixed (S,Se) second shell at 4.16 Å and a third shell of Cd atoms at 5.05–5.10 Å. In our case, we do not observe differences in the Se-Se and Se-S bond lengths of the second shell, whereas Ramos et al. [59] report a difference of about 0.1 Å. The Se-poorer  $21080_{\text{Se}=0.14}/437_{\text{Se}=0.12}$  and the Se-richer  $21150_{\text{Se}=0.47}/440_{\text{Se}=0.47}$  pigments share identical parameters within

**Fig. 4** Cd L<sub>3</sub>-edge XANES spectra recorded from **a** commercial and **b** historical CdS<sub>1-x</sub>Se<sub>x</sub> pigment powders. **c**, **d** Insets of the energy range indicated by the rectangles in **a**, **b**



**Fig. 5** **a**  $k^*$ -weighted Se K-edge EXAFS spectra in  $k$  space and **b** corresponding Fourier transforms in the range  $k = [2-16]$  Å<sup>-1</sup> of commercial (solid line) and historical (dotted line) CdS<sub>1-x</sub>Se<sub>x</sub> pigment powders



**Table 2** Quantitative analysis results of the Se-K edge XAS data of commercial and historical  $\text{CdS}_{1-x}\text{Se}_x$  pigment powders.  $x_S$  represents the sulfur content in the second coordination shell following the overall composition. Data were fitted in  $r$  space in the interval  $r = [1-3] \text{ \AA}$  after transformation of  $k^*x(k)$  data in the interval  $k = [2-16] \text{ \AA}^{-1}$ . The use of  $k$  weighting in place of the usual  $k^2$  or  $k^3$  was necessary to evidence the higher coordination shells. In all cases the  $\sigma^2_{\text{S,Se}}$  was fixed to the value found in sample 21080 $_{\text{Se}=0.14}$  ( $0.017 \text{ \AA}^{-2}$ )

Sample	$r_{\text{Cd}}$ ( $\text{\AA}$ )	$\sigma^2_{\text{Cd}}$ ( $\text{\AA}^2$ )	$x_S$	$r_S$ ( $\text{\AA}$ )	$r_{\text{Se}}$ ( $\text{\AA}$ )	$r_{\text{Cd}}$ ( $\text{\AA}$ )	$\sigma^2_{\text{Cd}}$ ( $\text{\AA}^2$ )
21080 $_{\text{Se}=0.14}$	$2.60 \pm 0.01$	$0.0053 \pm 0.0002$	$1.01 \pm 0.05$	$4.15 \pm 0.02$	–	$5.04 \pm 0.03$	$0.07 \pm 0.02$
437 $_{\text{Se}=0.12}$	$2.60 \pm 0.01$	$0.0053 \pm 0.0002$	$1.03 \pm 0.05$	$4.16 \pm 0.02$	–	$5.05 \pm 0.03$	$0.08 \pm 0.03$
21150 $_{\text{Se}=0.47}$	$2.61 \pm 0.01$	$0.0055 \pm 0.0002$	$0.59 \pm 0.05$	$4.16 \pm 0.03$	$4.16 \pm 0.03$	$5.09 \pm 0.03$	$0.05 \pm 0.02$
440 $_{\text{Se}=0.47}$	$2.61 \pm 0.01$	$0.0055 \pm 0.0002$	$0.60 \pm 0.06$	$4.18 \pm 0.03$	$4.16 \pm 0.03$	$5.10 \pm 0.03$	$0.05 \pm 0.01$

the error bars, meaning that the two  $\text{CdS}_{1-x}\text{Se}_x$  pigments with a comparable Se content have an identical structure. In line with the XRPD and EDX results (Table 1) the former pair is almost pure CdS, whereas the latter pair exhibits a content of Se of *ca.* 0.4.

To summarize, the results above-described prove that the morphology, microstructure and local atomic structure of  $\text{CdS}_{1-x}\text{Se}_x$  compounds depend only on the Se content. For a specific  $x_{\text{Se}}$ , such parameters do not affect the positions of the DLE bands and cannot be correlated with the changes observed in the relative intensity of DLE<sub>1</sub> and DLE<sub>2</sub>.

### 3.2.2 (Photo)chemical reactivity of $\text{CdS}_{1-x}\text{Se}_x$

To evaluate the effect of the Se content and of different environmental parameters on the overall degradation process of  $\text{CdS}_{1-x}\text{Se}_x$  in the oil binder, thus on their possible effects on the emission vis–NIR spectral properties of the pigment itself, we then studied a series of artificially aged oil paint mock-ups (Table 3). These samples, prepared using the set of commercial  $\text{CdS}_{1-x}\text{Se}_x$  pigment powders above-described (Table 1), were subjected to accelerated aging under UVA-vis light at RH ~ 30%, UVA-vis light at RH ≥ 95%, and thermal aging at  $T = 40^\circ$  and RH ≥ 95% (denoted as “UVA-vis<sub>RH30%</sub>”, “UVA-vis<sub>RH95%</sub>” and “thermal<sub>RH95%</sub>”, respectively). The optical and molecular changes induced by different aging treatments at the paint surface of all mock-ups were assessed by vis–NIR and colorimetric investigations, followed by ATR mode FT-IR spectroscopy and XRPD analyses. A summary of the results obtained from all the artificially aged paint mock-ups is reported in Table 3. In the following, a selection of the most meaningful results for the discussion is given.

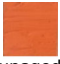







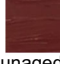



Regardless from the type of aging, colorimetric measurements (Table 3) show that the total color change ( $\Delta E^*$ ) is slightly perceptible with the naked eye ( $\leq 5$ ) for all paints.

In the corresponding diffuse reflectance vis spectra (black lines and insets in Fig. 6a and Supplementary Information: Fig. S7) a red shift of the absorption edge from *ca.* 567 nm (for 21080 $_{\text{Se}=0.14}$ ) to *ca.* 655 nm (for 21150 $_{\text{Se}=0.47}$ ) is observed, representing the sharpening of the band gap with increasing Se content. In line with the colorimetric results, spectra of all aged samples (magenta, red and grey lines in Fig. 6a and Supplementary Information: Fig. S7) show minor variations within the experimental error due to possible changes of the geometry of the instrumental set-up.

Photoluminescence spectra (black lines in Fig. 6b and Supplementary Information: Fig. S8) show a weak narrow emission in the visible range (below 700 nm) due to the contribution of NBE band, modified by the presence of the binder [16], and two broad emissions in the red-NIR region attributed to the DLE bands. In line with previous research [2, 16] and findings from historical paintings (Fig. 1), a bathochromic shift of these bands is observed with increasing Se content (e.g., for the DLE<sub>1</sub>: from *ca.* 780 to *ca.* 880 nm). As previously commented, any variation of the NBE can't be taken into account due to the overlapping with the binder emission (magenta, red and grey lines in Fig. 6b and Supplementary Information: Fig. S8). More revealing information can be obtained via analysis of the DLE bands. With aging, a general intensity decrease of the fluorescence is observed for all samples (result not shown). Whereas, no meaningful changes are observable in the spectra obtained from mock-ups photo-aged at RH ~ 30% (Supplementary Information: Fig. S8, red lines), variations are visible in those recorded from thermally aged paints (Supplementary Information: Fig. S8, grey lines) and samples aged by UVA-vis light at RH ≥ 95% (Fig. 6b, magenta lines). Changes in the relative intensity and red-shifts in position of the DLE bands are more pronounced for the photoaged paints at RH ≥ 95% and become gradually more evident with decreasing Se content (Fig. 6b and Supplementary Information: Figs. S8b and S9). According to previous studies [30, 31], the existence and relative intensity of the DLE<sub>1</sub> and DLE<sub>2</sub> bands has been attributed to the concentration of lattice-vacancy type defects ( $V_{\text{Se}}$ ) and oxygen-containing species incorporated in the vacancies, respectively. Thus, our findings suggest that the thermal treatment and the photoaging at RH ≥ 95% have introduced changes in the original distribution and concentration of crystal defects of  $\text{CdS}_{1-x}\text{Se}_x$  (i.e., vacancies and/or oxygen species incorporated in the vacancies) as result of the interaction between the surface of pigment particles, the binding medium and moisture.

In the most altered photoaged paints, specific information on the chemical nature of alteration products arising from the oxidative degradation of both the oil binder and the cadmium red pigment is highlighted by ATR FT-IR spectroscopy (Fig. 7) and XRPD investigations (Table 3).

**Table 3** Photographs and colorimetric, emission vis–NIR, FT-IR (ATR mode) and XRPD results obtained from  $\text{CdS}_{1-x}\text{Se}_x$  oil paint mock-ups before and after different aging conditions (for further details, see: Sect. 2.3, Figs. 6 and 7 and Supplementary Information: Figs. S7–S10)

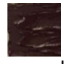
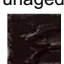
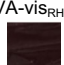

Sample/aging protocol <sup>a</sup>	Color change	Emission vis–NIR	FT-IR (ATR mode)	XRPD <sup>b</sup>
21080 <sub>Se=0.14</sub>	 unaged	–	Lipidic material (oil), BaSO <sub>4</sub>	CdS <sub>0.86</sub> Se <sub>0.14</sub> BaSO <sub>4</sub> (2.5 ± 0.1)
	 UVA-vis <sub>RH30%</sub>	As unaged sample	Oxidation products of the oil	As unaged sample
	 UVA-vis <sub>RH95%</sub>	Shift of DLE <sub>1</sub> band towards higher wavelengths (+ 17 nm); change of DLE <sub>1</sub> and DLE <sub>2</sub> relative intensity	Zinc oxalate; <sup>c</sup> cadmium sulfate	ZnC <sub>2</sub> O <sub>4</sub> ·2H <sub>2</sub> O (ca. 1–2%); CdSO <sub>4</sub> ·H <sub>2</sub> O (weak); probably Zn/Cd stearate or another carboxylate
	 thermal <sub>RH95%</sub>	Slight change of DLE <sub>1</sub> and DLE <sub>2</sub> relative intensity	Oxalate (possibly of Zn); <sup>c</sup> oxidation products of the oil	ZnC <sub>2</sub> O <sub>4</sub> ·2H <sub>2</sub> O (very weak, at the limit of detection)
	–	–	–	–
	 unaged	–	Lipidic material (oil), BaSO <sub>4</sub>	CdS <sub>0.78</sub> Se <sub>0.22</sub> BaSO <sub>4</sub> (very weak, at the limit of detection)
	 UVA-vis <sub>RH30%</sub>	As unaged sample	Oxidation products of the oil, possible oxalates (very weak)	As unaged sample
	 UVA-vis <sub>RH95%</sub>	Shift of DLE <sub>1</sub> band towards higher wavelengths (+ 6 nm); slight change of DLE <sub>1</sub> and DLE <sub>2</sub> relative intensity	Zinc oxalate; <sup>c</sup> cadmium sulfate	ZnC <sub>2</sub> O <sub>4</sub> ·2H <sub>2</sub> O (weak)
	 thermal <sub>RH95%</sub>	As unaged sample	Oxalate (possibly of Zn); <sup>c</sup> oxidation products of the oil	As unaged sample
	–	–	–	–
	 unaged	–	Lipidic material (oil), BaSO <sub>4</sub>	CdS <sub>0.64</sub> Se <sub>0.36</sub> (28.8 ± 0.1) CdS <sub>0.60</sub> Se <sub>0.40</sub> (71.2 ± 0.1)
	 UVA-vis <sub>RH30%</sub>	As unaged sample	Oxidation products of the oil, possible oxalates (very weak)	As unaged sample
	 UVA-vis <sub>RH95%</sub>	Small shift of DLE <sub>1</sub> band towards higher wavelengths (+ 3 nm); slight change of DLE <sub>1</sub> and DLE <sub>2</sub> relative intensity	Zinc oxalate <sup>c</sup>	ZnC <sub>2</sub> O <sub>4</sub> ·2H <sub>2</sub> O (very weak)
	 thermal <sub>RH95%</sub>	As unaged sample	Oxalate (possibly of Zn); <sup>c</sup> oxidation products of the oil	unidentified phase (very weak)

FT-IR spectra show the presence of new signals in the 1000–1200 cm<sup>−1</sup> range and below 650 cm<sup>−1</sup>, both ascribable to CdSO<sub>4</sub>·H<sub>2</sub>O [ $\nu_{1/3}(\text{SO}_4^{2-})$  and  $\nu_4(\text{SO}_4^{2-})$ , respectively]. Such bands are clearly visible for the Se-poorest sample (21080<sub>Se=0.14</sub>), barely appreciable in the mock-ups containing 0.2 < x<sub>Se</sub> < 0.4 (21100<sub>Se=0.22</sub> and 21130<sub>Se=0.39</sub>) and not appreciable in the Se-richest paint (21150<sub>Se=0.47</sub>). In addition, for all mock-ups, the formation of ZnC<sub>2</sub>O<sub>4</sub>·2H<sub>2</sub>O is pointed out by the IR bands at about 1630, 1364, 1317, 818 cm<sup>−1</sup>. This compound is the result of the reaction between Zn-species arising from impurities present in the original pigment formulation (as detected by XRF; results not shown) and the oxalate ions arising from the oxidative degradation of the oil [63, 64]. Overall, the degradation phenomenon manifests itself as a visible chalking and loss of gloss of the paint surface, similarly to that already earlier observed for cadmium yellow paints [37, 65].

In line with the FT-IR analysis, XRPD investigations (Table 3), allowed crystalline ZnC<sub>2</sub>O<sub>4</sub>·2H<sub>2</sub>O to be identified in all UVA-vis<sub>RH95%</sub> aged samples, while it permitted to detect CdSO<sub>4</sub>·H<sub>2</sub>O only in the aged paint 21080<sub>Se=0.14</sub>. A series of broad signals at low 2θ angles are possibly attributable to unidentified long chain metal carboxylates. For those mock-ups that contain two CdS<sub>1-x</sub>Se<sub>x</sub>



**Table 3** continued

Sample/aging protocol <sup>a</sup>	Color change	Emission vis–NIR	FT-IR (ATR mode)	XRPD <sup>b</sup>
21150 <sub>Se=0.47</sub>  unaged  UVA-vis <sub>RH30%</sub>  UVA-vis <sub>RH95%</sub>  thermal <sub>RH95%</sub>	–	–	Lipidic material (oil), BaSO <sub>4</sub>	CdS <sub>0.55</sub> Se <sub>0.45</sub> (35.0 ± 0.1) CdS <sub>0.45</sub> Se <sub>0.55</sub> (57.9 ± 0.1) BaSO <sub>4</sub> (7.1 ± 0.1)
	ΔE* = 2 ± 1 ΔL* = 1 ± 1 Δa* = – 1.5 ± 0.9 Δb* = – 0.4 ± 0.5	As unaged sample	Oxidation products of the oil	As unaged sample
	ΔE* = 1 ± 1 ΔL* = 0.5 ± 0.9 Δa* = – 0.4 ± 0.7 Δb* = 0.3 ± 0.4	As unaged sample	Zinc oxalate <sup>c</sup>	ZnC <sub>2</sub> O <sub>4</sub> ·2H <sub>2</sub> O (very weak)
	ΔE* = 2 ± 3 ΔL* = 1 ± 2 Δa* = – 2 ± 2 Δb* = 1 ± 1	As unaged sample	Oxalate (possibly of Zn); <sup>c</sup> oxidation products of the oil	As unaged sample

<sup>a</sup>See ref [2] for further details about the optical, molecular spectroscopy and crystalline structure results of the powders

<sup>b</sup>Values in brackets refer to the weight percentage of each phase obtained by Rietveld refinement of the XRPD pattern

<sup>c</sup>Traces of Zn were detected by XRF in the powders (results not reported)

<sup>d</sup>The value of  $x_{Se}$ , reported as subscript in the name of each sample, was obtained as weighted average of the  $x_{Se}$  of the two CdS<sub>1–x</sub>Se<sub>x</sub> phases (*cf.* Table 1)

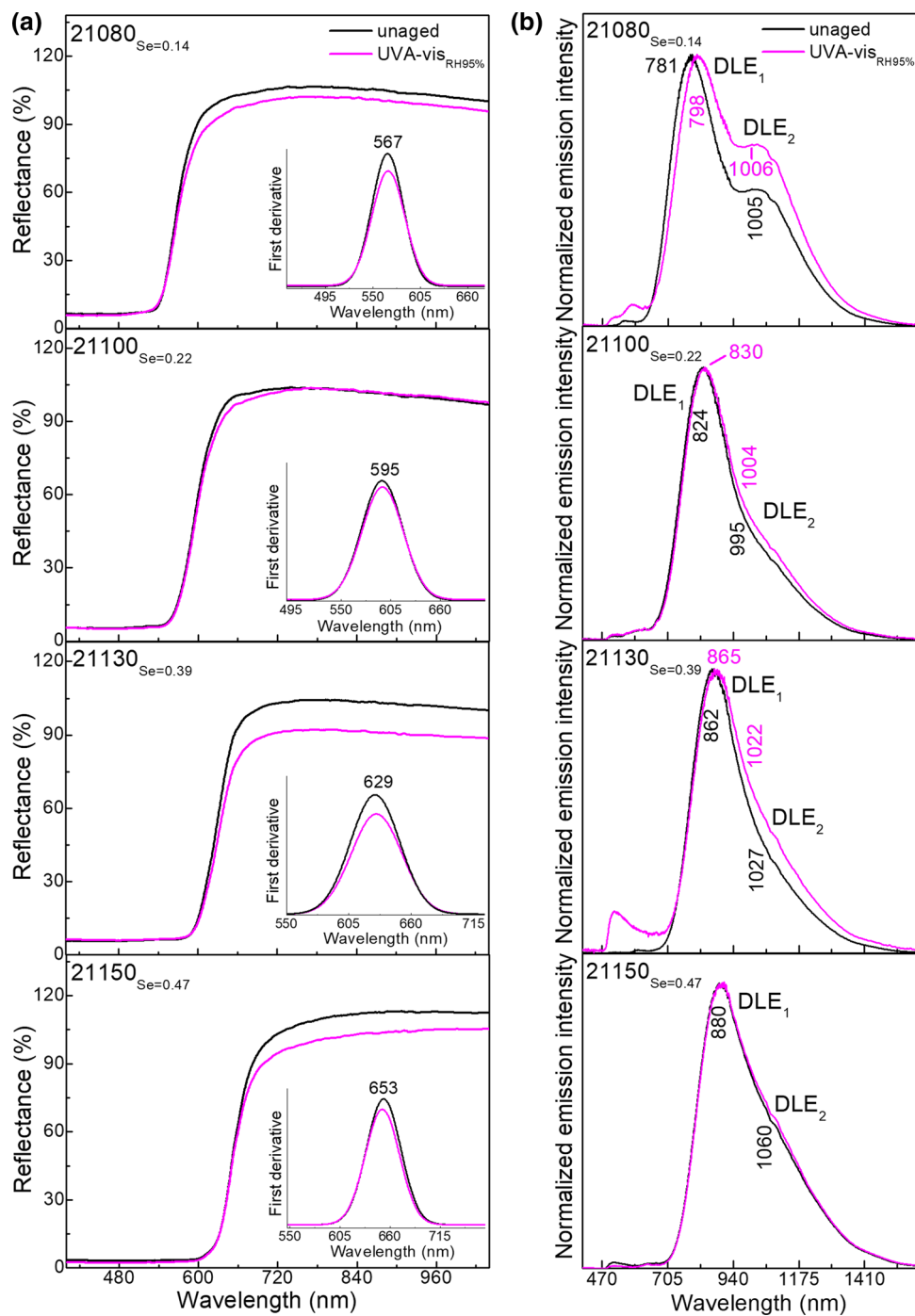
phases (i.e., 21130<sub>Se=0.39</sub> and 21150<sub>Se=0.47</sub>), it appears that the aging treatment does not produce any change on the relative peak intensities, meaning that the relative amounts of the two phases remain unchanged. This is reasonably expected due to the relatively slight difference in the Se content of the two phases that are present together in the same sample (namely,  $x_{Se} = 0.36$  and 0.40 for 21130<sub>Se=0.39</sub>;  $x_{Se} = 0.45$  and 0.55 for 21150<sub>Se=0.47</sub>; see Table 1).

It is noteworthy that the photoaging at RH ~ 30% and the thermal treatment did not promote the formation of secondary compounds associated to the oxidation of CdS<sub>1–x</sub>Se<sub>x</sub> pigments, but mainly chemical changes related to the oxidative degradation of the oil (Table 3 and Supplementary Information: Fig. S10).

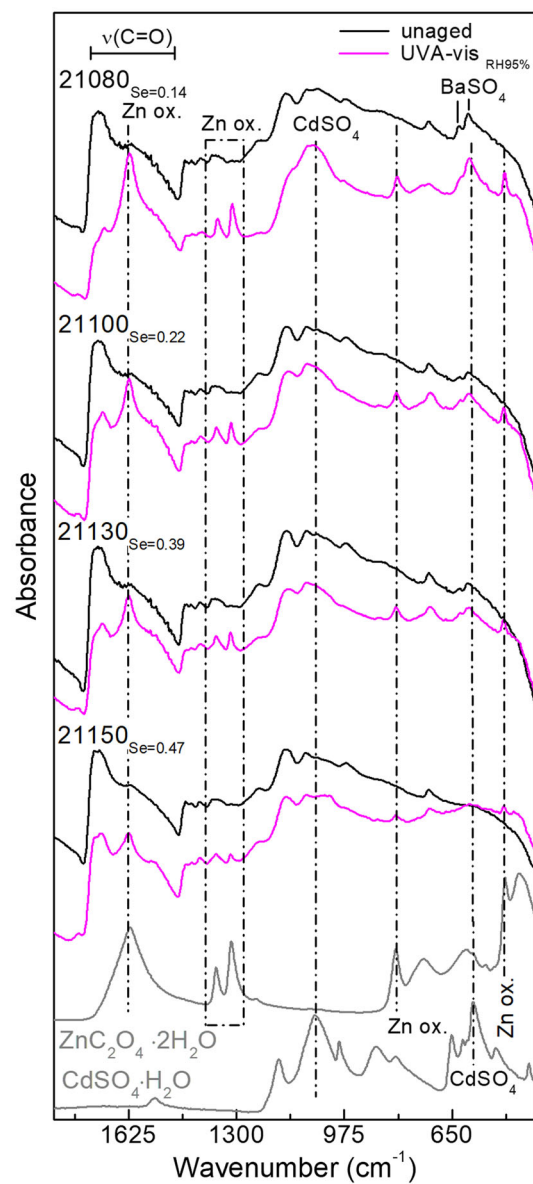
To evaluate the role of the oil in the photodegradation process of the pigment under high moisture levels, we have also investigated equivalent pellets made up of only the cadmium reds (i.e., not mixed with linseed oil). With respect to the oil mock-up aged under similar conditions (*cf.* Figs. 6 and 7), reflection mode FT-IR spectroscopy investigations of pellet 21080<sub>Se=0.14</sub> (Fig. 8a) reveal that in the absence of the oil binder the formation of cadmium sulfate has not occurred. Such observation was further supported by XRPD investigations (results not shown). The emission vis–NIR spectrum (Fig. 8b) shows similar but less pronounced changes as observed for the equivalent oil paint mock-up: the enhancement of the DLE<sub>2</sub> band and a red-shift of DLE<sub>1</sub> band. This result further support the hypothesis on the possible role of moisture in affecting the relative intensity of DLE bands also in the absence of meaningful modifications of the pigment chemical composition.

To summarize, our findings show that red CdS<sub>1–x</sub>Se<sub>x</sub> compounds show tendency to convert to white CdSO<sub>4</sub>·H<sub>2</sub>O under exposure to UVA-visible light at high moisture conditions (RH ~ 95%) but not at environmental humidity (RH ~ 30%). We also found that the photo-oxidation process is triggered by the presence of the oil binder and it becomes more and more evident as the substitution fraction of selenium decreases, being more favoured for the Se-poorest varieties of CdS<sub>1–x</sub>Se<sub>x</sub> ( $x_{Se} \sim 0.1$ –0.2), compounds that exhibit a higher photocatalytic activity for the oil oxidation. Moreover, moisture is one of the possible external factors influencing the relative intensity of the DLE bands.

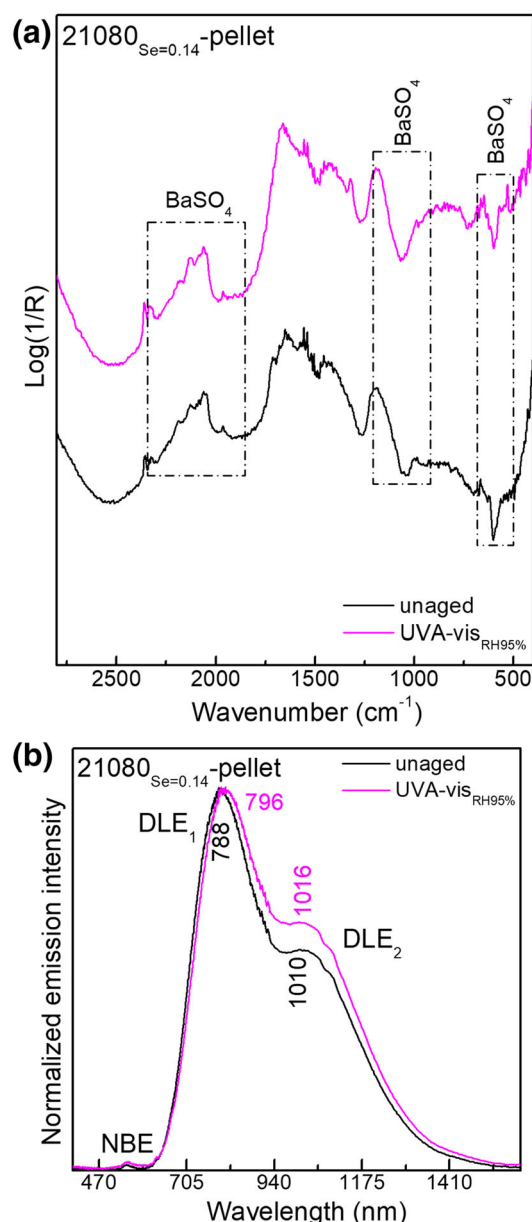
**Fig. 6** **a** Diffuse reflectance vis spectra and **b** normalized emission vis-NIR spectra of  $\text{CdS}_{1-x}\text{Se}_x$  oil paint mock-ups before (black) and after exposure to UVA-vis light and high moisture conditions ( $\text{RH} \geq 95\%$ ) (magenta)



**Fig. 7** ATR-mode FT-IR spectra recorded from  $\text{CdS}_{1-x}\text{Se}_x$  oil paint mock-ups before (black) and after exposure to UVA-vis light and high moisture conditions ( $\text{RH} \geq 95\%$ ) (magenta). In grey, spectra of selected reference compounds



**Fig. 8** **a** Reflection-mode FT-IR spectra and **b** normalized emission vis-NIR spectra recorded from commercial 21080<sub>Se=0.14</sub> pellet before (black) and after exposure to UVA-vis light and high moisture conditions ( $RH \geq 95\%$ ) (magenta)



### 3.3 Assessment of the conservation state of cadmium red areas in two paintings by J. Pollock

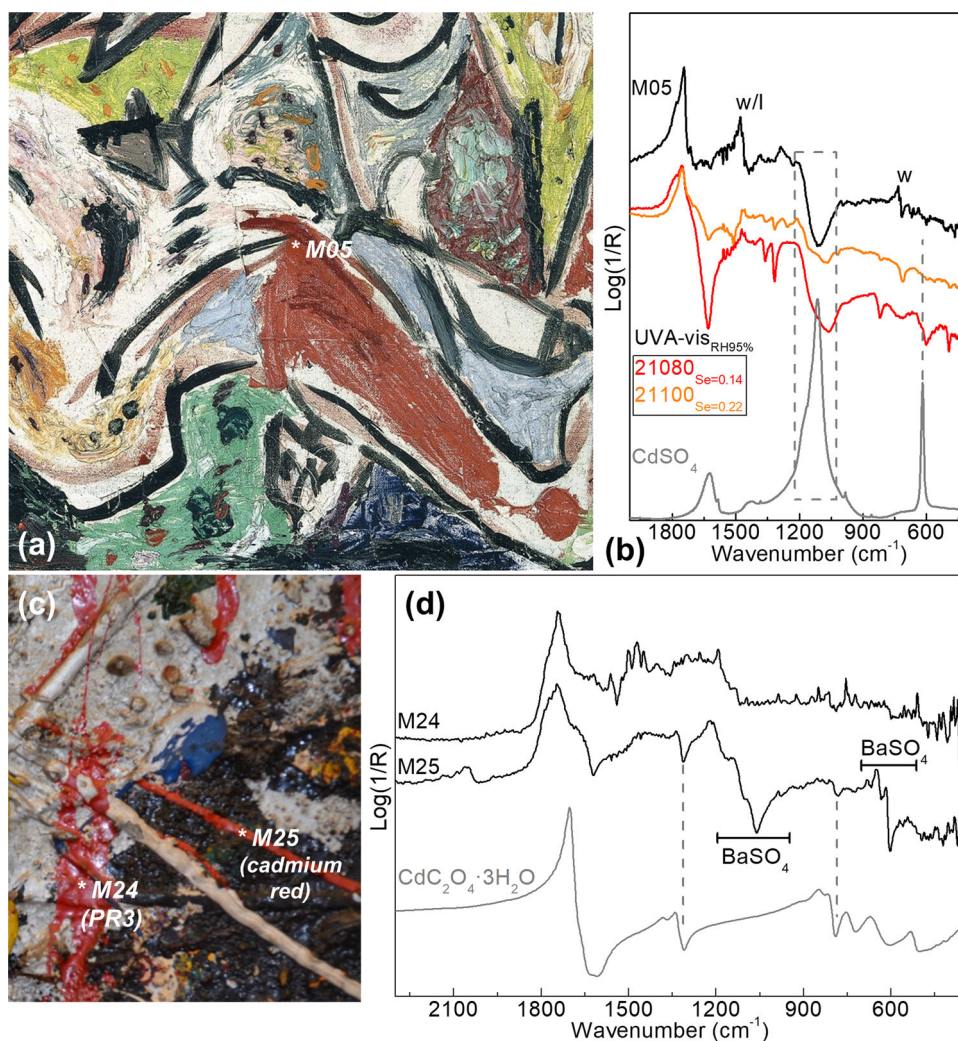
To untangle complexity on the conservation state of cadmium red-based paints in artworks, we have finally exploited the knowledge acquired from the artificially aged paint mock-ups for a thorough interpretation of the non-invasive reflection FT-IR results (Fig. 9) obtained from two of the paintings earlier analyzed by vis-NIR spectroscopy (Fig. 1), namely: *Alchemy* and *Bird Effort* by J. Pollock. The two case studies were selected for featuring  $\text{CdS}_{1-x}\text{Se}_x$  pigments with a similar Se content (Fig. 1;  $x_{\text{Se}} \approx 0.30\text{--}0.40$ ) and an intense DLE<sub>2</sub> band (*Bird Effort*, case 2-II: intensity DLE<sub>2</sub> > intensity DLE<sub>1</sub>; *Alchemy*, case 3: intensity DLE<sub>2</sub>  $\approx$  intensity DLE<sub>1</sub>).

In *Bird Effort*, the FT-IR spectrum (M05 in Fig. 9a, b) reveals the presence of a strong inverted band at about 1100  $\text{cm}^{-1}$  suggesting the presence of a sulfate compound. The good agreement between such spectral feature and the one obtained from the photo-aged paint mock-ups in which  $\text{CdSO}_4$  was identified (red and orange lines in Fig. 9b) suggests the presence of the same sulfate also in the investigated cadmium red-based areas of *Bird Effort*.

In *Alchemy*, as outlined by previous research [18], Pollock painted the red areas not only using cadmium red but also an organic pigment, namely an azo  $\beta$ -naphthol pigment Toluidine red (also known as PR3). Interestingly, FT-IR spectra (Fig. 9c, d) show the presence of cadmium oxalate only in correspondence of the opaque and thick  $\text{CdS}_{1-x}\text{Se}_x$ -based paint along with evident bands of  $\text{BaSO}_4$  (M25). The metal-oxalate compound is absent in the glossy red paint made of PR3 (M24) and is limited to the red thick lines composed of cadmium red.



**Fig. 9** **a** Detail of the painting *Bird Effort* depicting the red paint made of  $\text{CdS}_{1-x}\text{Se}_x$  ( $x_{\text{Se}} \approx 0.30\text{--}0.40$ ) and **b** reflection-mode FT-IR spectrum recorded on the cadmium red paint (black) compared with spectra of the aged UVA-vis<sub>RH95%</sub> 21080  $\text{Se}=0.14$  (red) and 21100  $\text{Se}=0.22$  (orange) oil paint mock-ups and  $\text{CdSO}_4$  (grey). w = long hydrocarbon chain-based material (paraffin, wax); l = lipid. **c** Detail of the painting *Alchemy* depicting two red paints: a glossy and very liquid one composed of the azo  $\beta$ -naphthol pigment Toluidine red (also known as PR3) and an opaque and thick one made up of  $\text{CdS}_{1-x}\text{Se}_x$  ( $x_{\text{Se}} \approx 0.30\text{--}0.40$ ). **d** Reflection-mode FT-IR spectra recorded on the two types of reds (black) compared with the reference spectrum of cadmium oxalate trihydrate (grey)



Overall, the comparison between the results arising from the study of artificially aged paint mock-ups with those recorded from historical paintings has allowed us to reasonably establish that the presence of cadmium sulfate and cadmium oxalate result from a degradation process of selected cadmium red paints of *Alchemy* and *Bird Effort*. Although the cadmium red paint areas of the two selected case studies show different photoluminescence properties, at the moment we cannot establish any correlation with the chemical reactivity of  $\text{CdS}_{1-x}\text{Se}_x$  paints.

### 3.4 Photo-oxidation pathway of $\text{CdS}_{1-x}\text{Se}_x$ oil paints upon UVA-vis illumination and variable moisture conditions

Within the bounds of our experiments on mock-ups, we have demonstrated that both moisture and the oil binder promote the photo-oxidation of  $\text{CdS}_{1-x}\text{Se}_x$  pigments to  $\text{CdSO}_4 \cdot \text{H}_2\text{O}$ . The process (known also as photodissolution/photocorrosion) takes place in association with the formation of organo-compounds (i.e., oxalates), thus pointing out the efficiency of  $\text{CdS}_{1-x}\text{Se}_x$ -based particles as photocatalysts for the oxidation of the binding medium. Based on the experimental findings discussed above and previous research in the context of cadmium yellow paints [37], environmental sciences and photocatalysis [1, 4, 40, 66, 67], a series of explanations can be provided to the photo-oxidation process of cadmium red oil paints under variable moisture conditions.

In a first step, electron-hole ( $e^-$ - $h^+$ ) pairs are produced under the supra-band gap light ( $h\nu > E_g$ ), illumination, with electrons that are excited to the conduction band. Afterwards, they can either recombine, by dissipating the absorbed light energy as heat or photons without promoting any chemical transformation, or migrate to the surface of particles, by starting a series of chemical reactions. For explaining the photochemical reactivity of cadmium reds in the oily binder, besides light absorption properties and bandgap energies of the pigment, also the valence band maximum (VBM) and conduction band minimum (CBM) energies with respect to the thermodynamic redox potential ( $\phi$ ) of both  $\text{CdS}_{1-x}\text{Se}_x$  and of water relative to NHE (normal hydrogen electrode) at pH 7 will be discussed. Although all these values are pH dependent and have been calculated in aqueous environment [68, 69],

we can consider them to be reliable due to the employed high moisture aging conditions and because in oil paintings the chemical environment is neutral/slightly acidic [70].

We found that, under exposure to light and high relative humidity conditions ( $RH \geq 95\%$ ), Se-poorer  $CdS_{1-x}Se_x$  pigments show a higher tendency towards photocorrosion than the Se-richer ones, as highlighted by the more efficient formation of  $CdSO_4 \cdot H_2O$  (Fig. 7 and Table 3). The result can be justified as follows. In general, a semiconductor is stable with respect to  $h^+$  oxidation if its thermodynamic oxidation potential ( $\phi^{ox}$ ) and its VBM are more positive than  $\phi(O_2/H_2O)$  (0.82 V) [68, 69]. We can reasonably assume that such conditions are not satisfied for the analyzed aged  $CdS_{1-x}Se_x$  compounds: (i) their VBM is more positive than  $\phi(O_2/H_2O)$ , with VBM energy values that become more and more positive with decreasing Se content [66, 67]; (ii)  $\phi^{ox}$  of  $CdSe/CdS_xSe_{1-x}$  is in general more negative than  $\phi(O_2/H_2O)$  [1, 4, 40, 69].

In addition, we have demonstrated that the photocatalytic efficiency of  $CdS_{1-x}Se_x$  increases with decreasing Se content, as established via the strong decrease of IR signals of the oil binder and the formation of oxalates (Fig. 7). The band gap energy ( $E_g$ ) progressively decreases from 21080<sub>Se=0.14</sub> (2.26 eV) to 21150<sub>Se=0.55</sub> (1.97 eV) (Supplementary Information: Table S4), such that the relative positions of CBM and VBM in the  $CdS_{1-x}Se_x$  compounds progressively shift toward more negative and positive values, respectively, with decreasing Se content. Elevation of the CBM with respect to the water reduction level  $\phi(2H^+/H_2) = -0.41$  V increases the thermodynamic drive force for water reduction [66, 67], thus enhancing the photocatalytic activity of Se-poorer  $CdS_{1-x}Se_x$  compounds for the oil oxidation. Under high moisture photoaging conditions, the oxidation of sulfide-species to  $CdSO_4 \cdot H_2O$  is more efficient when the  $CdS_{1-x}Se_x$  pigment is embedded in the oil paint matrix (*cf.* Figs. 7 and 8) due to the formation of radicals from the oil, which contribute to the photo-corrosion of CdS-compounds.

Similar to what was earlier observed for cadmium yellow paints [37], we established that the photo-oxidation process of  $CdS_{1-x}Se_x$  and its inefficiency as a photocatalyst is hindered at “regular” environmental relative humidity conditions ( $RH \sim 30\%$ ). This can be ascribed to the  $e^-h^+$  recombination efficiency, which is very likely the dominant deactivation pathway with decreasing moisture levels (Supplementary Information: Figs. S7a, S8a and S10a).

From the emission vis–NIR spectroscopy results appears also clear that aging treatments upon high moisture conditions influence the spectral properties of the vis–NIR DLE bands, by enhancing the intensity of the DLE<sub>2</sub> (Fig. 6b and Supplementary Information: Fig. S8b). Nevertheless, further research is required in order to elucidate what are the intrinsic factors of  $CdS_{1-x}Se_x$  (other than morphology, microstructure and local atomic structure; *cf.* Sect. 3.2.2) that are responsible for the differences observed in the relative intensity of the vis–NIR DLE bands.

## 4 Conclusions

A multi-length scale and multi-method approach has been presented here to expand knowledge of the photoluminescence properties and (photo)chemical reactivity of cadmium red ( $CdS_{1-x}Se_x$ )-based paints by combining non-invasive/non-destructive vis–NIR and vibrational spectroscopies at the macro-scale with advanced electron microscopy mapping and X-ray methods at the micron- and nano-scales.

The results obtained from the extensive study of artificially aged oil paint mock-ups and powders made up of  $CdS_{1-x}Se_x$  compounds with a variable Se content (with  $0.1 < x < 0.5$ ) permitted us to provide first evidence of the tendency of such class of compounds toward photo-degradation and to identify some of the key-factors driving the process. Within the boundaries of our experimental conditions, the investigation of mock-ups led us to draw the following conclusions:

- (i) The photodegradation of red  $CdS_{1-x}Se_x$  compounds occurs via the formation of  $CdSO_4 \cdot H_2O$ . This process is triggered by high moisture levels ( $RH \geq 95\%$ ) and by the presence of the oil binder. Under such circumstances,  $CdS_{1-x}Se_x$  acts also as a photocatalyst for the oil oxidation, leading to the formation of oxalates. Further research is still ongoing on Se-speciation with the aim to investigate and clarify the way in which selenium participates to the degradation pathways of  $CdS_{1-x}Se_x$  paints, via the possible formation of oxidized Se-compounds.
- (ii) At environmental moisture levels ( $\sim 30\%$  RH), electron–hole recombination becomes the dominant deactivation pathway, thus hindering the photo-oxidation in cadmium red paints.
- (iii) The photo-reactivity of cadmium red paints depends on the Se content and is more efficient for the Se-poorer  $CdS_{1-x}Se_x$  types. The depletion of Se in the  $CdS_{1-x}Se_x$  structure lowers the valence band maximum and raises the conduction band minimum. The former is responsible for the enhanced photo-oxidation of  $CdS_{1-x}Se_x$ , while the latter improves its photocatalytic activity.
- (iv) In dark and high moist conditions ( $RH \geq 95\%$ ) the transformation of sulfides into sulfates is inhibited. Oxalates were detected as secondary compounds of the thermal reaction between the pigment formulation and the oxidation products of the oil. The process is less efficient with respect to the one observed during photoaging treatment performed under similar humidity levels.

The combination of the findings from paint-mock-ups with the results from the non-invasive spectroscopy investigations of cadmium red-based areas in a series of twentieth century paintings led us to conclude that the observed cadmium sulfate and cadmium oxalate can be interpreted as alteration products of the analyzed historical paints. In addition, the high specificity of vis–NIR spectroscopy in providing information concerning the photoluminescence properties of  $CdS_{1-x}Se_x$  pigments, allowed us to classify the identified  $CdS_{1-x}Se_x$  pigments in three main groups, depending on the relative intensity of the two characteristic

deep-level emission (DLE) bands associated to crystal defects. Results obtained from the set of commercial and historical  $\text{CdS}_{1-x}\text{Se}_x$  powders showed that the particle morphology, microstructure and local structure of the pigment do not affect the relative intensity of DLEs. Changes in the spectral properties of these bands appear instead to be influenced by the presence of moisture. Such findings have opened the way for targeted research on the main intrinsic factors and other external parameters related to the manufacturing process of cadmium reds (e.g., temperature) that may affect the characteristic vis–NIR photoluminescence of  $\text{CdS}_{1-x}\text{Se}_x$  powders with a similar Se content and any eventual correlation with their (photo)chemical reactivity. Studies are still underway and their results will be published in a follow-up paper.

To summarize, we consider that our findings provide deeper insights into the photoluminescence properties of  $\text{CdS}_{1-x}\text{Se}_x$  as well as important hints about the degradation mechanism of cadmium red paints, by contributing to the optimization of preventive conservation strategies of a series of twentieth century paintings. The alteration of cadmium red paints leads to an overall color change of the surface that is difficult to perceive with the naked eye; however, care should be taken, since the degradation process promotes to the formation of more mobile and (partially) soluble compounds, such as sulfates. Remarkably, the alteration of the cadmium red paints can be mitigated using similar conditions as earlier proposed for cadmium yellows [24, 37], namely: (i) minimization of the exposure of the painting to moisture (i.e.,  $\text{RH}\% < 40\%$ ); (ii) maintenance of illumination conditions at the regular values foreseen for lightfast painting materials [71].

**Supplementary Information** The online version contains supplementary material available at <https://doi.org/10.1140/epjp/s13360-022-02447-7>.

**Acknowledgements** Authors acknowledge M. Duranti, A. Baffoni, F. Duranti and the staff of Civic Museum of Palazzo della Penna of Perugia together with Assessorato alla Cultura del Comune di Perugia to give the permission for investigating the paintings *Lago Umbro* and *Incendio Città* by G. Dottori and for publishing their photographic details. A special thanks also to the entire staff of the Peggy Guggenheim Collection in Venice and the Musée Picasso in Antibes for their support during the analysis of the paintings by J. Pollock and N. de Staël and to Dr. David Buti of CATS in Copenhagen for having provided the historical cadmium red pigment powders.

**Funding** The research was financially supported by the EU FP7 and Horizon 2020 Projects CHARISMA (FP7-INFRASTRUCTURES, GA No. 228330), IPERION-CH (H2020-INFRAIA-2014-2015, GA No. 654028), IPERION-HS (H2020-INFRAIA-2019-1, GA No. 871034) and ESTEEM3 (Research and innovation programme, GA No. 823717) and the Italian project AMIS (Dipartimenti di Eccellenza 2018–2022, funded by MIUR and Perugia University). For the beamtime grants received, we thank ESRF-ID21 (Experiment No. HG156 and in-house beamtimes) and the CERIC-ERIC Research Infrastructure for the investigations at ESRF-BM08 (LISA) beamline (Proposal Id: 20207042). D.C. acknowledges TOP/BOF funding of the University of Antwerp.

**Data Availability Statement** This manuscript has associated data in a data repository. [Authors' comment: The data sets generated during and/or analyses during the current study are available from the corresponding authors on reasonable request].

## Declarations

**Conflict of interest** Authors declare that they have no conflicts of interest.

**Open Access** This article is licensed under a Creative Commons Attribution 4.0 International License, which permits use, sharing, adaptation, distribution and reproduction in any medium or format, as long as you give appropriate credit to the original author(s) and the source, provide a link to the Creative Commons licence, and indicate if changes were made. The images or other third party material in this article are included in the article's Creative Commons licence, unless indicated otherwise in a credit line to the material. If material is not included in the article's Creative Commons licence and your intended use is not permitted by statutory regulation or exceeds the permitted use, you will need to obtain permission directly from the copyright holder. To view a copy of this licence, visit <http://creativecommons.org/licenses/by/4.0/>.

## References

1. R. Xie, J. Su, Y. Liu, L. Guo, *Int. J. Hydrog. Energy* **39**, 3517 (2014). <https://doi.org/10.1016/j.ijhydene.2013.12.088>
2. C. Grazia, F. Rosi, F. Gabrieli, A. Romani, M. Paolantoni, R. Vivani, B.G. Brunetti, P. Colomban, C. Miliani, *Microchem. J.* **125**, 279 (2016). <https://doi.org/10.1016/j.microc.2015.11.008>
3. R.H. Bube, *J. Appl. Phys.* **35**, 586 (1964). <https://doi.org/10.1063/1.1713421>
4. D. Long, M. Li, D. Meng, R. Ahuja, Y. He, *J. Appl. Phys.* **123**, 105103 (2018). <https://doi.org/10.1063/1.5018381>
5. Q. Zhang, X. Xing, X. Zhou, X. Xiong, T. Zhai, *Adv. Opt. Mater.* **5**, 1600877 (2017). <https://doi.org/10.1002/adom.201600877>
6. S.N. Moger, M.G. Mahesha, *J. Alloys Compd.* **870**, 159479 (2021). <https://doi.org/10.1016/j.jallcom.2021.159479>
7. U. Woggon, S.V. Gaponenko, *Phys. Status Solidi B* **189**, 285 (1995). <https://doi.org/10.1002/pssb.2221890202>
8. A. Uhrig, L. Banyai, S. Gaponenko, A. Wörner, N. Neuroth, C. Klingenshirn, *Zeitschrift für Physik D Atoms Mol. Clust.* **20**, 345 (1991). <https://doi.org/10.1007/BF01544007>
9. A.A. Yadav, E.U. Masumdar, *J. Alloys Compd.* **505**, 787 (2010). <https://doi.org/10.1016/j.jallcom.2010.06.141>
10. I. Fiedler, M. Bayard, in *Artist's Pigments, A Handbook of their History and Characteristics*, vol. 1, ed. by R.L. Feller (National Gallery of Art, Washington, 1986), p. 65
11. A. Martins, C. Albertson, C. McGlinchey, J. Dik, *Herit. Sci.* **4**, 22 (2016). <https://doi.org/10.1186/s40494-016-0091-4>
12. C. Miliani, A. Sgamellotti, K. Kahrim, B.G. Brunetti, A. Aldrovandi, M.R. van Bommel, K.J. van den Berg, H. Janssen, in *ICOM Committee for Conservation. Triennial meeting, 15th, New Delhi, India, 2008*, ed. By J. Bridgland (Allied Publishers Pvt. Ltd., New Delhi, Mumbai, Kolkata, 2008), p. 857
13. K. Muir, A. Langley, A. Bezur, F. Casadio, J. Delaney, G. Gautier, *J. Am. Inst. Conserv.* **52**, 156 (2013)



14. J. Lee, B. Ormsby, A. Burnstock, K.J. van Den Berg, in *Conservation of Modern Oil Paintings*, ed. By K. Jan van den Berg, I. Bonaduce, A. Burnstock, B. Ormsby, M. Scharff, L. Carlyle, G. Heydenreich, K. Keune (Springer, Cham, 2019), p. 495. [https://doi.org/10.1007/978-3-030-19254-9\\_38](https://doi.org/10.1007/978-3-030-19254-9_38)
15. F. Rosi, M. Patti, L. Cartechini, F. Gabrieli, L. Monico, A. Romani, C. Anselmi, A. Daveri, A. Sgamellotti, C. Milani, in *Gerardo Dottori: The Futurist View*, ed. by M. Duranti, A. Baffoni, F. Duranti (Fabrizio Fabbri Editore, Perugia, 2014), p. 33
16. C. Grazia, C. Sapienza, C. Miliani, A. Romani, in *UV-Vis Luminescence Imaging Techniques*, ed. By M. Picollo, M. Stols-Witlox, L. F. López (Editorial Universitat Politècnica de València, 2019), p. 181
17. E. O'Donoghue, A.M. Johnson, J. Mazurek, F. Preusser, M. Schilling, M.S. Walton, *Stud. Conserv.* **51**(sup2), 62 (2006). <https://doi.org/10.1179/sic.2006.51.Supplement-2.62>
18. F. Rosi, C. Grazia, R. Fontana, F. Gabrieli, L. Pensabene Buemi, E. Pampaloni, A. Romani, C. Stringari, C. Miliani, *Herit. Sci.* **4**, 18 (2016). <https://doi.org/10.1186/s40494-016-0089-y>
19. A. Perchuk, A. Phenix, L. Rivers, *Getty Res. J.* **9**(S1), 27 (2017)
20. R. Elovich, *The Burlington Magazine* **691**, (1981)
21. F. Rosi, C. Miliani, C. Clementi, K. Kahrim, F. Presciutti, M. Vagnini, V. Manuali, A. Daveri, L. Cartechini, B.G. Brunetti, A. Sgamellotti, *Appl. Phys. A Mater. Sci. Process.* **100**, 613 (2010). <https://doi.org/10.1007/s00339-010-5744-7>
22. F. Pozzi, J. Arslanoglu, F. Carò, C. Stringari, *Appl. Phys. A Mater. Sci. Process.* **122**, 917 (2016). <https://doi.org/10.1007/s00339-016-0435-7>
23. P. Molaro, C. Caliri, D. Pavone, F.P. Romano, *J. Cult. Herit.* **47**, 265 (2021). <https://doi.org/10.1016/j.culher.2020.09.014>
24. L. Monico, L. Cartechini, F. Rosi, A. Chieli, C. Grazia, S. De Meyer, G. Nuyts, F. Vanmeert, K. Janssens, M. Cotte, W. De Nolf, G. Falkenberg, I. Crina Anca Sandu, E. Storevik Tveit, J. Mass, R. Pereira de Freitas, A. Romani, C. Miliani, *Sci. Adv.* **6**, (2020). <https://doi.org/10.1126/sciadv.aay3514>
25. W.G. Huckle, G.F. Swigert, S.E. Wiberley, *Ind. Eng. Chem. Prod. Res. Dev.* **5**, 362 (1966). <https://doi.org/10.1021/i360020a016>
26. J. Wu, K. Li, X. Xu, Y. Zhang, X. Xu, X. Lao, J. Wuhan Univ. Technol. Mat. Sci. Edit. **30**, 1247 (2015). <https://doi.org/10.1007/s11595-015-1303-6>
27. M. Thoury, J.K. Delaney, E.R. de la Rie, M. Palmer, K. Morales, J. Krueger, *Appl. Spectrosc.* **65**, 939 (2011). <https://doi.org/10.1366/11-06230>
28. A. Romani, C. Clementi, C. Miliani, G. Favaro, *Acc. Chem. Res.* **43**, 837 (2010). <https://doi.org/10.1021/ar900291y>
29. V. Babentsov, J. Riegler, J. Schneider, O. Ehler, T. Nann, M. Fiederle, J. Cryst. Growth **280**, 502 (2005). <https://doi.org/10.1016/j.jcrysgro.2005.03.086>
30. M.J.S. Brasil, P. Motisuke, F. Decker, J.R. Moro, *J. Phys. C Solid State Phys.* **21**, 3141 (1988). <https://doi.org/10.1088/0022-3719/21/16/024>
31. A. Urbietta, P. Fernández, J. Piqueras, *J. Appl. Phys.* **96**, 2210 (2004). <https://doi.org/10.1063/1.1765858>
32. F. Rosi, C. Grazia, F. Gabrieli, A. Romani, M. Paolantoni, R. Vivani, B.G. Brunetti, P. Colomban, C. Miliani, *Microchem. J.* **124**, 856 (2016). <https://doi.org/10.1016/j.microc.2015.07.025>
33. M. Ghirardello, S. Mosca, J. Marti-Rujas, L. Nardo, A. Burnstock, A. Nevin, M. Bondani, L. Toniolo, G. Valentini, D. Comelli, *Anal. Chem.* **90**, 10771 (2018). <https://doi.org/10.1021/acs.analchem.8b01666>
34. M. Ghirardello, V. Otero, D. Comelli, L. Toniolo, D. Dellasega, L. Nessi, M. Cantoni, G. Valentini, A. Nevin, M.J. Melo, *Dyes Pigm.* **186**, 108998 (2021). <https://doi.org/10.1016/j.dyepig.2020.108998>
35. C. Miliani, L. Monico, M.J. Melo, S. Fantacci, E.M. Angelin, A. Romani, K. Janssens, *Angew. Chem. Int. Ed.* **57**, 7324 (2018). <https://doi.org/10.1002/anie.201802801>
36. D. Comelli, D. MacLennan, M. Ghirardello, A. Phenix, C.M. Schmidt Patterson, H. Khanjian, M. Gross, G. Valentini, K. Trentelman, A. Nevin, *Anal. Chem.* **91**, 3421 (2019). <https://doi.org/10.1021/acs.analchem.8b04914>
37. L. Monico, A. Chieli, S. De Meyer, M. Cotte, W. de Nolf, G. Falkenberg, K. Janssens, A. Romani, C. Miliani, *Chem. Eur. J.* **24**, 11584 (2018). <https://doi.org/10.1002/chem.201801503>
38. J.B. Katari, V.L. Colvin, A.P. Alivisatos, *J. Phys. Chem.* **98**, 4109 (1994). <https://doi.org/10.1021/j100066a034>
39. D.A. Hines, M.A. Becker, P.V. Kamat, *J. Phys. Chem. C* **116**, 13452 (2012). <https://doi.org/10.1021/jp303659g>
40. H. Liu, H. Gao, M. Long, H. Fu, P. Alvarez, Q. Li, S. Zheng, X. Qu, D. Zhu, *Environ. Sci. Technol.* **51**, 6877 (2017). <https://doi.org/10.1021/acs.est.7b00654>
41. G. Rayner, S.D. Costello, A. McClelland, A. Akey, K. Eremin, *Heritage* **4**, 1497 (2021). <https://doi.org/10.3390/heritage4030082>
42. L. Monico, K. Janssens, M. Cotte, A. Romani, L. Sorace, C. Grazia, B.G. Brunetti, C. Miliani, *J. Anal. At. Spectrom.* **30**, 1500 (2015). <https://doi.org/10.1039/C5JA00091B>
43. J. Schindelin, I. Arganda-Carreras, E. Frise, V. Kaynig, M. Longair, T. Pietzsch, S. Preibisch, C. Rueden, S. Saalfeld, B. Schmid, J. Tinevez, D.J. White, V. Hartenstein, K. Eliceiri, P. Tomancak, A. Cardona, *Nat. Methods* **9**, 676 (2012). <https://doi.org/10.1038/nmeth.2019>
44. C. Larson, R.B. Von Dreele, Generalized Structure Analysis System (GSAS), Los Alamos National Laboratory Report LAUR 86-748 (2004)
45. D. Balzar, N. Audebrand, M. Daymond, A. Fitch, A. Hewat, J.I. Langford, A. Le Bail, D. Louër, O. Masson, C.N. McCowan, N.C. Popa, P.W. Stephens, B.J. Toby, *Appl. Crystallogr.* **37**, 911 (2004). <https://doi.org/10.1107/S0021889804022551>
46. M. Cotte, E. Pouyet, M. Salome, C. Rivard, W. De Nolf, H. Castillo-Michel, T. Fabris, L. Monico, K. Janssens, T. Wang, P. Sciau, L. Verger, L. Cormier, O. Dargaud, E. Brun, D. Bugnazet, B. Fayard, B. Hesse, A.P. del Real, G. Veronesi, J. Langlois, N. Balcar, Y. Vandenberghe, V.A. Sole, J. Kieffer, R. Barrett, C. Cohen, C. Cornu, R. Baker, E. Gagliardini, E. Papillon, J. Susini, *J. Anal. At. Spectrom.* **32**, 477 (2017). <https://doi.org/10.1039/C6JA00356G>
47. F. d'Acapito, G.O. Lepore, A. Puri, A. Laloni, F. La Manna, E. Dettona, A. De Luisa, A. Martin, *J. Synchrotron Radiat.* **26**, 551 (2019). <https://doi.org/10.1107/S160057751801843X>
48. P. Raimondi, *Synchrotron Radiat. News* **29**, 8 (2016). <https://doi.org/10.1080/08940886.2016.1244462>
49. S. Fisher, M. Oscarsson, W. De Nolf, M. Cotte, J. Meyer, *J. Synchrotron Radiat.* (2021). <https://doi.org/10.1107/S1600577521009851>
50. B. Ravel, M. Newville, *J. Synchrotron Radiat.* **12**, 537 (2005). <https://doi.org/10.1107/S0909049505012719>
51. A.L. Ankudinov, B. Ravel, J.J. Rehr, S.D. Conradson, *Phys. Rev. B* **58**, 7565 (1998). <https://doi.org/10.1103/PhysRevB.58.7565>
52. G. Kresse, J. Furthmüller, *Phys. Rev. B* **54**, 11169 (1996). <https://doi.org/10.1103/PhysRevB.54.11169>
53. L. Bertrand, S. Schöeder, D. Anglos, M.B. Breese, K. Janssens, M. Moini, A. Simon, *TrAC Trends Anal. Chem.* **66**, 128 (2015). <https://doi.org/10.1016/j.trac.2014.10.005>
54. C. Gervais, M. Thoury, S. Réguer, P. Gueriau, J. Mass, *Appl. Phys. A Mater. Sci. Process.* **121**, 945 (2015). <https://doi.org/10.1007/s00339-015-9462-z>
55. M. Gano, E.S. Pouyet, S.M. Webb, C.M. Schmidt Patterson, M.S. Walton, *Pure Appl. Chem.* **90**, 463 (2018). <https://doi.org/10.1515/pac-2017-0502>
56. L. Monico, M. Cotte, F. Vanmeert, L. Amidani, K. Janssens, G. Nuyts, J. Garrevoet, G. Falkenberg, P. Glatzel, A. Romani, C. Miliani, *Anal. Chem.* **92**, 14164 (2020). <https://doi.org/10.1021/acs.analchem.0c03251>
57. F. Rosi, A. Daveri, B. Doherty, S. Nazzareni, B.G. Brunetti, A. Sgamellotti, C. Miliani, *Appl. Spectrosc.* **64**, 956 (2010). <https://doi.org/10.1366/000370210792080975>
58. M. Aceto, A. Agostino, G. Fenoglio, A. Idone, M. Gulmini, M. Picollo, P. Ricciardi, J.K. Delaney, *Anal. Methods* **6**, 1488 (2014). <https://doi.org/10.1039/C3AY41904E>
59. A. Ramos, C. Levelut, J. Petiau, F. Villain, *J. Phys. Condens. Matter* **5**, 3507 (1993). <https://doi.org/10.1088/0953-8984/5/22/004>
60. A. Ramos, C. Levelut, J. Petiau, *Mater. Sci. Eng. B* **9**, 425 (1991). [https://doi.org/10.1016/0921-5107\(91\)90066-5](https://doi.org/10.1016/0921-5107(91)90066-5)



61. C. Levelut, A. Ramos, J. Petiau, M. Robino, Mater. Sci. Eng. B **8**, 251 (1991). [https://doi.org/10.1016/0921-5107\(91\)90045-W](https://doi.org/10.1016/0921-5107(91)90045-W)
62. Y.M. Yiu, M.W. Murphy, L. Liu, Y. Hu, T.K. Sham, AIP Conf. Proc. **1590**, 26 (2014). <https://doi.org/10.1063/1.4870191>
63. M.W. Murphy, Y.M. Yiu, M.J. Ward, L. Liu, Y. Hu, J.A. Zapien, Y. Liu, T.K. Sham, J. Appl. Phys. **116**, 193709 (2014). <https://doi.org/10.1063/1.4902390>
64. K.P. Simonsen, J.N. Poulsen, F. Vanmeert, M. Ryhl-Svendsen, J. Bendix, J. Sanyova, K. Janssens, F. Mederos-Henry, Herit. Sci. **8**, 126 (2020). <https://doi.org/10.1186/s40494-020-00467-z>
65. F. Rosi, L. Cartechini, L. Monico, F. Gabrieli, M. Vagnini, D. Buti, B. Doherty, C. Anselmi, B. G. Brunetti, C. Miliani, in *Metal Soaps in Art*, ed. By. F. Casadio, K. Keune, P. Noble, A. van Loon, E. Hendriks, S. Centeno, G. Osmond (Springer, Cham, 2019) p. 173. [https://doi.org/10.1007/978-3-319-90617-1\\_10](https://doi.org/10.1007/978-3-319-90617-1_10)
66. B. Leone, A. Burnstock, C. Jones, P. Hallebeek, J. Boon, K. Keune, in *ICOM Committee for Conservation. Triennial Meeting, 14th, The Hague, Netherlands, 2005* (James & James, London, 2005) p. 803
67. M. de los Angeles Hernandez-Perez, E. A. Sanchez-Ramirez, F. J. Castillo-Plata, A. Manzo-Robledo, J. R. Aguilar-Hernandez, A. Ezeta-Mejia, J. Sastre-Hernandez, E. Ramirez-Meneses, M. Villanueva-Ibañez, A. A. Flores-Caballero, Vacuum **175**, 109277 (2020). <https://doi.org/10.1016/j.vacuum.2020.109277>
68. H. S. Jung, J. Joo, K. Lee, Y. T. Kang, J. CO<sub>2</sub> Util. **52**, 101671 (2021). <https://doi.org/10.1016/j.jcou.2021.101671>
69. S. Chen, L. W. Wang, Chem. Mater. **24**, 3659 (2012). <https://doi.org/10.1021/cm302533s>
70. W. Anaf, O. Schalm, K. Janssens, K. De Wael, Dyes Pigm. **113**, 409 (2015). <https://doi.org/10.1016/j.dyepig.2014.09.015>
71. R. Wolbers, *Cleaning Painted Surfaces: Aqueous Methods* (Archetype, London, 2000)
72. Commission Internationale de L'Eclairage, Control of Damage to Museum Objects by Optical Radiation (The Commission, Vienna, Austria, 2004) ISBN: 978 3 901906 27 5